Mixed-Metal Hybrid Polyoxometalates with Amino Acid Ligands: Electronic Versatility and Solution Properties

Fateme Akhlaghi Bagherjeri,[†] Michele Vonci,[†] Edward A. Nagul,[†] Chris Ritchie,[†] Robert W. Gable,[†] Matthew B. Taylor, Gary Bryant, Si-Xuan Guo, Jie Zhang, Pablo A. Aparicio, Xavier Lopez, Josep M. Poblet,[‖] and Colette Boskovic*[,†]

[†]School of Chemistry, University of Melbourne, Parkville, Victoria 3010, Australia

[§]School of Science, RMIT University, Melbourne, Victoria 3001, Australia

[‡]School of Chemistry, Monash University, Clayton, Victoria 3800, Australia

[‖]Departament de Quımica Fısica i Inorganica, Universitat Rovira i Virgili, Marcel·lí Domingo 1, 43007 Tarragona, Spain

* Supporting Information

ABSTRACT: Eight new members of a family of mixed-metal (Mo,W) polyoxometalates (POMs) with amino acid ligands have been synthesized and investigated in the solid state and solution using multiple physical techniques. While the peripheral POM structural framework is conserved, the different analogues vary in nuclearity of the central metal−oxo core, overall redox state, metal composition, and identity of the zwitterionic α-amino acid ligands. Structural investigations reveal site-selective substitution of Mo for W, with a strong preference for Mo to occupy the central metal−oxo core. This core structural unit is a closed tetrametallic loop in the blue reduced species and an open trimetallic loop in the colorless oxidized analogues. Density functional theory calculations suggest the core as the favored site of reduction and reveal that the corresponding molecular orbital is much lower in energy for a tetra- versus trimetallic core. The reduced species are diamagnetic, each with a pair of strongly antiferromagnetically coupled Mo^{V} centers in the tetrametallic core, while in the oxidized complexes all Mo is hexavalent. Solution small-angle X-ray scattering and circular dichroism (CD) studies indicate that the hybrid POM is stable in aqueous solution on a time scale of days within defined concentration and pH ranges, with the stability enhanced by the presence of excess amino acid. The CD experiments also reveal that the amino acid ligands readily exchange with other α-amino acids, and it is possible to isolate the products of amino acid exchange, confirming retention of the POM framework. Cyclic voltammograms of the reduced species exhibit an irreversible oxidation process at relatively low potential, but an equivalent reductive process is not evident for the oxidized analogues. Despite their overall structural similarity, the oxidized and 2e-reduced hybrid POMs are not interconvertible because of the respective open- versus closed-loop arrangement in the central metal−oxo cores.

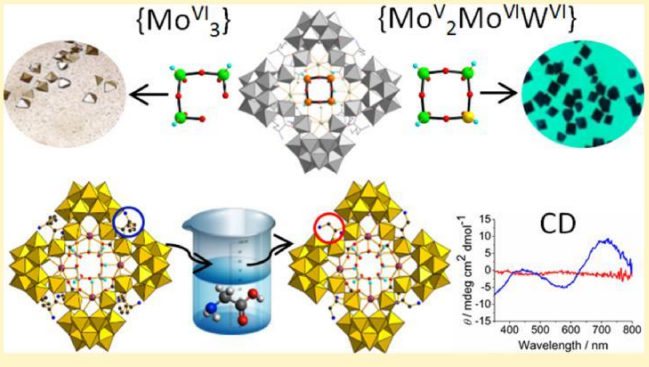

INTRODUCTION

For over 100 years, the qualitative and quantitative colorimetric analysis of phosphates, arsenates, and similar species has been based on the characteristic “molybdenum blue” color of some reduced polyoxometalates (POMs).[1] Underlying these applications, as well as applications in oxidation catalysis,[2] is the extensive redox chemistry displayed by many of these molecular analogues of metal oxides.[3] Their ability to reversibly accept multiple electrons also confers on POMs a capacity to act as multielectron reservoirs or transfer agents. Promise for the development of novel electronic materials or water oxidation catalysts for green energy production is thus evident for hybrid compounds that result from covalently attaching redox-active POMs to other moieties with electronic or catalytic activity.[4,5] Polyoxometalate redox chemistry is correlated with photo-activity involving photoreduction of the POM in the presence of organic electron donors[6,7] or by water at an interface.[8] Reduced POMs can act as chemical reductants,[9] including photoreduced POMs acting as catalysts for water reduction or the formation of precious metal nanoparticles.[10−13] In some cases other metal complexes are required as photosensitizers. The facility of reduction of a particular POM depends on factors including the charge to nuclearity ratio and therefore the identity and oxidation state of the heteroatoms.[14−17] Poly-oxomolybdates are more readily reduced than are isostructural polyoxotungstates, and the Mo atoms are preferentially reduced in mixed-metal Mo/W POMs.[18] Notable reduced POMs are the mixed-valence molybdenum blue Mo^{V}/Mo^{VI} “giant wheels” based on {Mo_{154}} units,[19−21] which are obtained by partial

reduction of Mo^{VI} solutions at pH <3. Molybdenum blues are reduced by an even number of electrons with the reducing electrons delocalized in pairs over well-defined parts of the POM, resulting in diamagnetism.[22−26] For instance, the {Mo154} wheel has 28 Mo^{V} centers. While the giant Mo wheels and other mixed-valence polyoxomolybdates are often air-stable, the "heteropoly blue" reduced forms of polyoxotungstates are typically air-sensitive.

Tuning the redox, catalytic, and other properties of POMs can be achieved by varying the POM composition through several means, including the incorporation of other metal centers, organic ligands, or metal−ligand complexes.[27−34] However, characterization of the resulting species can be challenging, particularly in the case of mixed-valence, mixed-metal compounds, with the application of multiple comple-mentary physical techniques sometimes necessary, even to simply determine the compound formulation. In the case of mixed-metal species, determination of the number and structural positions of the different metal centers can often be achieved through single-crystal X-ray diffraction, complemented by elemental analysis. For mixed-valence species, the questions that arise concern first the number of reducing electrons and second the location and degree of delocalization of these electrons. Crystallography can give insights into the valence of the metal centers, as can EPR and X-ray photoelectron spectroscopy (XPS), while magnetometry can indicate the number of unpaired electrons. In solution, redox titrations, electrochemistry, and UV−visible spectroelectrochemistry are most useful for determining the exact degree of reduction. Computational chemistry has also become increasingly accurate and affordable in terms of computation time, and the insights provided are invaluable for elucidating the electronic structure of POMs and hybrid POMs.[14,15]

Solution speciation studies have established that POMs interconvert in solution, depending especially on pH and POM concentration.[3] Thus, before conclusions can be drawn from chemical or physical properties observed in solution, it is essential to ascertain the identity and stability of the complex in solution, which will also depend on factors such as overall ionic strength, organic solvent, and presence of other species. Multinuclear ^{51}V and ^{183}W NMR has been used extensively in this regard, especially for high-symmetry polyoxovanadates or polyoxotungstates.[35,36] Mass spectrometry can indicate the composition of the POM in the gas phase and by implication in the solution that was injected into the spectrometer.[37] A technique for investigating the solution structure or solution stability of POMs that has become more prevalent recently is small-angle X-ray scattering (SAXS), which can give information about the size and shape of discrete POMs, assemblies of POMs, or POM-containing ion pairs or clusters in solution.[36,38−43] Polyoxometalates as small as $[Nb_6O_{19}]^{8-}$ have been characterized by SAXS.[44] Also relevant to this work is the issue of chirality, as POMs can be dissymmetric and thus intrinsically chiral or chirality can be induced in nominally achiral POMs through covalent binding or electrostatic association of chiral organic moieties.[45−53]

We recently communicated the first two members of a new family of mixed-metal hybrid polyoxometalates with amino acid ligands (Figure 1) of general formula $[As_4(M_4)Mo^{VI}_xW^{VI}_{44-x}Y_4O_{160}(AA)_y(H_2O)_z]^{n-}$ (M = combination of Mo, W, and Y; AA = α-amino acid; x = 0−3; y = 8, 9).[54] Using p-methylbenzylammonium (p-$MeBzNH_3^+$) cations and glycine (Gly) or enantiopure L- or D-norleucine (L-Nle or D-Nle) amino acid ligands (Chart 1), we were able to access structural analogues formulated as $(p\text{-}MeBzNH_3)_6K_2(GlyH)$ $[As_4(YW^{VI}_3)W^{VI}_{44}Y_4O_{159}(Gly)_8(H_2O)_{14}]\cdot 47H_2O$ (1) and enantiomorphs $(p\text{-}MeBzNH_3)_{15}(NleH)_3[As_4(Mo^{V}_2Mo^{VI}_2)W^{VI}_{44}Y_4O_{160}(Nle)_9(H_2O)_{11}][As_4(Mo^{VI}_2W^{VI}_2)W^{VI}_{44}Y_4O_{160}(Nle)_9(H_2O)_{11}]$ (generically designated 2: L-Nle, 2a; D-Nle, 2b), which together illustrate the structural versatility of this family of compounds. The common yttrium polyoxotungstate framework of 1 and 2 is reminiscent of that of the long-known $[As_4W_{40}O_{140}]^{28-}$ and its lanthanoid derivatives, as well as the more recently reported $[Ln_6(H_2O)_{22}\{As_4W_{44}(OH)_2(proline)_2O_{151}\}]^{10-}$.[55−58] The zwitterionic amino acid ligands of 1 and 2 bridge the metal centers via carboxylate groups, with the protonated amine groups involved in intramolecular hydrogen bonding to the POM. This framework supports an inner oxo-bridged tetrametallic {M_4} "core" (M = Mo, W, Y), and density functional theory (DFT) calculations revealed that the first two reducing electrons are always delocalized on this {M_4} core and are strongly antiferromagnetically coupled. The resulting diamagnetism was confirmed by magnetic susceptibility and EPR measurements. The diamagnetic compound 2 is thus comprised of an equal mixture of fully oxidized and 2e-reduced POMs. The structural versatility that is evident from 1 and 2 includes (i) preferential metal substitution of Mo for W in the {M_4} core, (ii) site-selective reduction of the {M_4} core, (iii) the ability to access chiral analogues using chiral amino acid ligands, and (iv) the accessibility of different crystal-packing motifs and solubility properties through varying the ligand− cation combination. Although 1 is essentially insoluble, SAXS, electrospray ionization mass spectrometry (ESI-MS), electronic

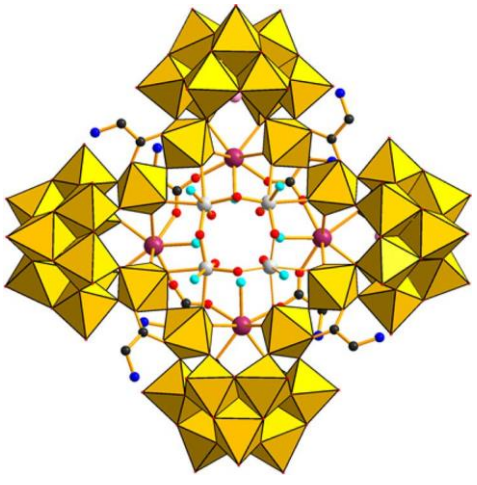

Figure 1. Structural representation of the idealized hybrid polyoxometalate $[As_4(M^{VI}_4)W^{VI}_{44}Y_4O_{160}(Gly)_8(H_2O)_{12}]^{8-}$ (M = Mo, W). Color code: WO_6 octahedra, yellow; Y, violet; disordered Mo/W, gray; As, pink; C, black; N, dark blue; O, red; aqua ligands, cyan.

Chart 1

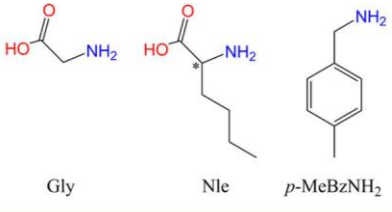

absorption and CD spectroscopy, and electrochemical studies of 2 established structural retention of the POM backbone in DMSO and/or Nle buffer (pH 2.2) on a time scale of at least 1 day, although the presence or absence of amino acid ligand exchange was not determined conclusively. Compound 2 was obtained following photoreduction by UV light and is essentially an equal mixture of oxidized and 2e-reduced analogues. To fully elucidate the properties of this family of hybrid POMs, our aims with the present work were 3-fold: (i) to obtain a fully 2e reduced $\{Mo^{V}_2\}$-containing analogue of 2, rather than a mixture of complexes with different degrees of reduction, (ii) to achieve complete Mo substitution of the four metal sites in the central tetrametallic core, and (iii) to elucidate the nature of amino acid ligand exchange in solution.

EXPERIMENTAL SECTION

Synthesis. All manipulations were performed under aerobic conditions, using materials as received. The precursor $K_{14}[As_2W_{19}O_{67}(H_2O)]$ was prepared as described previously.[59]

(p-MeBzNH$_3$)$_7$(L-NleH)$_5$[As$_4$(Mo$^{VI}_3$)Mo$^{VI}_{2.5}$W$^{VI}_{41.5}$Y$_4$O$_{159}$(L-Nle)$_8$(H$_2$O)$_{11}$]·20H$_2$O (3). Solid $K_{14}[As_2W_{19}O_{67}(H_2O)]$ (0.5263 g, 0.1000 mmol) was dissolved in 0.2 M L-norleucine solution (15 mL, 3.0 mmol) at pH 2.2, with this pH maintained during the dissolution by addition of concentrated HCl (37%). To this solution was added $Na_2MoO_4{\cdot}2H_2O$ (0.050 g, 0.20 mmol) while the pH was maintained at 2.2 using 3 M HCl. Solid $Y(NO_3)_3{\cdot}6H_2O$ (0.0626 g, 0.163 mmol) was then added, and the pH of the resulting solution was once again adjusted to 2.2. After the reaction mixture was allowed to stand for 1 h, p-MeBzNH$_2$ (50 μL, 0.39 mmol) was added and the reaction solution was wrapped in foil and stored in the dark. Colorless tetrahedral-shaped crystals formed overnight in 15% yield (100 mg, 0.007 mmol) based on W. Structural analysis by X-ray crystallography afforded the formula (p-MeBzNH$_3$)$_7$(L-NleH)$_5$[As$_4$(Mo$^{VI}_3$)Mo$^{VI}_{2.5}$W$^{VI}_{41.5}$Y$_4$O$_{159}$(L-Nle)$_8$(H$_2$O)$_{11}$]·78H$_2$O (3w) for the wet crystals, which partially dehydrate upon drying. Anal. Calcd (found) for air-dried 3, $C_{134}H_{320}N_{20}As_4Mo_{5.5}W_{41.5}Y_4O_{216}$: C, 11.11 (11.3); H, 2.23 (2.3); N, 1.93 (2.0); As, 2.07 (2.0); Y, 2.46 (2.4); Mo 3.64 (3.3). Selected IR (KBr, cm^{-1}): 1731 (w), 1621 (s), 1500 (w), 1456 (w), 1432 (w), 1382 (w), 1339 (w), 955 (m), 859 (s), 805 (m), 720(m), 610 (s), 4821(w), 458 (w). ^{1}H NMR (400 MHz, D$_2$O): δ 0.92 (t, J = 8.0 Hz, 39H, CH$_3$), 1.39 (m, 52H, (CH$_2$)$_2$), 1.90 (m, 26H, CH$_2$), 2.38 (s, 21H, CH$_3$), 3.85 (t, J = 6.0 Hz, 13H, CH), 4.18 (s, 14H, CH$_2$), 7.33, 7.40 ppm (ABq, J = 8.0 Hz, 28H, ArH). ^{13}C{^{1}H} NMR (800 MHz, D$_2$O): δ 13.6 (CH$_3$), 21.0 (CH$_3$), 22.3 (CH$_2$), 27.0 (CH$_2$), 30.6 (CH2), 43.7 (CH$_2$), 55.0 (CH), 129.6, 130.3, 130.4, 140.3 (Ar), 174.9 ppm (COO).

(p-MeBzNH$_3$)$_7$(L-NleH)$_3$[As$_4$(Mo$^{V}_2$Mo^{VI}W^{VI})Mo$^{VI}_x$W$^{VI}_{44-x}$Y$_4$O$_{160}$-(L-Nle)$_9$(H$_2$O)$_{11}$]·L-Nle·20H$_2$O (x = 1.5 (4a), 2 (4b), 2.5 (4c)). Solid $K_{14}[As_2W_{19}O_{67}(H_2O)]$ (0.5263 g, 0.1000 mmol) was dissolved in 0.2 M norleucine (L-Nle, 4a–c) solution (15 mL, 3.0 mmol) at pH 2.2, with this pH being maintained during the dissolution by addition of concentrated HCl (37%). To this solution was added $Na_2MoO_4{\cdot}2H_2O$ (0.040 g, 0.16 mmol) while the pH at 2.2 was maintained using 3 M HCl. Solid $Y(NO_3)_3{\cdot}6H_2O$ (0.0626 g, 0.163 mmol) was then added and the pH of the resulting solution was once again adjusted to 2.2. After the reaction mixture was allowed to stand for 1 h, hydrazinium sulfate solution (0.10 M; 200 μL, 0.02 mmol, 4a; 400 μL, 0.04 mmol, 4b; 800 μL, 0.08 mmol, 4c) was added and the solution left overnight. To the resulting dark blue solution was added p-MeBzNH$_2$ (50 μL, 0.39 mmol). Deep blue tetrahedral-shaped crystals formed over the course of several days, and one or two further crops could be collected after several weeks. Although all crops were spectroscopically identical, all of the physical studies reported herein were performed on the first crop.

(p-MeBzNH$_3$)$_7$(L-NleH)$_3$[As$_4$(Mo$^{V}_2$Mo^{VI}W^{VI})Mo$^{VI}_{1.5}$W$^{VI}_{42.5}$Y$_4$O$_{160}$(L-Nle)$_9$(H$_2$O)$_{11}$]·L-Nle·20H$_2$O (4a). Structural analysis by X-ray crystallography afforded the formula (p-MeBzNH$_3$)$_7$(L-NleH)$_3$[As$_4$(Mo$^{V}_2$Mo^{VI}W^{VI})Mo$^{VI}_{1.5}$W$^{VI}_{42.5}$Y$_4$O$_{160}$(L-Nle)$_9$(H$_2$O)$_{11}$]·L-Nle·75H$_2$O (4aw) for the wet crystals, which partially dehydrate upon drying. Yield: 150 mg, 0.011 mmol (23% based on W). Anal. Calcd (found) for air-dried 4a, $C_{134}H_{318}N_{20}As_4Mo_{4.5}W_{43.5}Y_4O_{217}$: C, 10.90 (11.4); H, 2.17 (2.2); N, 1.90 (1.9); As, 2.03 (1.98); Y, 2.41 (2.4); Mo 2.92 (2.6). Selected IR (KBr, cm^{-1}): 1731 (w), 1624 (s), 1496 (m), 1460 (w), 1430 (w), 1379 (w), 1344 (w), 955 (m), 861 (s), 808 (m), 765(m), 490 (w), 456 (w). ^{1}H NMR as per 4b.

(p-MeBzNH$_3$)$_7$(L-NleH)$_3$[As$_4$(Mo$^{V}_2$Mo^{VI}W^{VI})Mo$^{VI}_2$W$^{VI}_{42}$Y$_4$O$_{160}$(L-Nle)$_9$(H$_2$O)$_{11}$]·L-Nle·20H$_2$O (4b). Structural analysis by X-ray crystallography afforded the formula (p-MeBzNH$_3$)$_7$(L-NleH)$_3$[As$_4$(Mo$^{V}_2$Mo^{VI}W^{VI})Mo$^{VI}_2$W$^{VI}_{42}$Y$_4$O$_{160}$(L-Nle)$_9$(H$_2$O)$_{11}$]·L-Nle·83H$_2$O (4bw) for the wet crystals, which partially dehydrate upon drying. Yield: 160 mg, 0.011 mmol (25% based on W). Anal. Calcd (found) for air-dried 4b, $C_{134}H_{318}N_{20}As_4Mo_5W_{43}Y_4O_{217}$: C, 10.93 (11.2); H, 2.18 (2.2); N, 1.90 (1.9); As, 2.04 (2.1); Y, 2.42 (2.4); Mo 3.26 (3.1). Selected IR (KBr, cm^{-1}): 1731 (w), 1617 (s), 1494 (w), 1456 (w), 1430 (w), 1382 (w), 1344 (w), 955 (m), 895 (s), 856 (s), 810 (m), 781 (m), 737 (s), 765 (m), 671 (s), 637 (s), 490 (w), 456 (w). ^{1}H NMR (400 MHz, D$_2$O): δ 0.92 (m, 39H, CH$_3$), 1.38 (m, 52H, (CH$_2$)$_2$), 1.91 (m, 26H, CH$_2$), 2.38 (s, 21H, CH$_3$) 3.82 (t, J = 6.4 Hz, 13H, CH), 4.19 (s, 14H, CH$_2$), 7.33, 7.40 ppm (ABq, J = 8.4 Hz, 28H, ArH). ^{13}C{^{1}H} NMR (800 MHz, D$_2$O): δ 13.6 (CH$_3$), 20.9 (CH$_3$), 22.3 (CH$_2$), 27.0 (CH$_2$), 30.5 (CH2), 43.7 (CH$_2$), 54.9 (CH), 129.6, 130.3, 130.4, 140.3 (Ar), 174.8 ppm (COO).

(p-MeBzNH$_3$)$_7$(L-NleH)$_3$[As$_4$(Mo$^{V}_2$Mo^{VI}W^{VI})Mo$^{VI}_{2.5}$W$^{VI}_{41.5}$Y$_4$O$_{160}$(L-Nle)$_9$(H$_2$O)$_{11}$]·L-Nle·20H$_2$O (4c). Structural analysis by X-ray crystallography afforded the formula (p-MeBzNH$_3$)$_7$(L-NleH)$_3$[As$_4$(Mo$^{V}_2$Mo^{VI}W^{VI})Mo$^{VI}_{2.5}$W$^{VI}_{41.5}$Y$_4$O$_{160}$(L-Nle)$_9$(H$_2$O)$_{11}$]·L-Nle·69H$_2$O (4cw) for the wet crystals, which partially dehydrate upon drying. Yield: 165 mg, 0.011 mmol (25% based on W). Anal. Calcd (found) for air-dried 4c, $C_{134}H_{318}N_{20}As_4Mo_{5.5}W_{42.5}Y_4O_{217}$: C, 10.96 (11.3); H, 2.18 (2.3); N, 1.91 (2.0); As, 2.04 (2.1); Y, 2.42 (2.4); Mo 3.59 (3.2). Selected IR (KBr, cm^{-1}): 1731 (w), 1614 (s), 1459 (w), 1440 (m), 1432 (w), 1381 (w), 1344 (w), 952 (m), 893 (s), 856 (s), 813 (m), 760(s), 736 (s), 669 (s), 640 (s), 487 (w), 452 (w). ^{1}H NMR as per 4b.

(p-MeBzNH$_3$)$_4$(DL-NleH)$_5${[As$_4$(Mo$^{V}_2$Mo^{VI}W^{VI})W$^{VI}_{44}$Y$_4$O$_{160}$(DL-Nle)$_8$(H$_2$O)$_{12}$]$_{0.5}$[As$_4$(Mo$^{VI}_3$W^{VI})W$^{VI}_{44}$Y$_4$O$_{160}$(DL-Nle)$_8$(H$_2$O)$_{12}$]$_{0.5}$}·DL-Nle·35H$_2$O (5). Synthesized as per 4b using DL-Nle in place of L-Nle, resulting in very thin square platelike crystals overnight. Yield: 200 mg, 0.014 mmol (31% based on W). Anal. Calcd (found) for $C_{116}H_{329}N_{18}As_4Mo_3W_{45}Y_4O_{235}$: C, 9.32 (9.5); H, 2.22 (2.1); N, 1.69 (1.8); As, 2.00 (1.9); Y, 2.38 (2.9); Mo 1.92 (2.0). Selected IR (KBr, cm^{-1}): 1727 (w), 1619 (s), 1491 (w), 1456 (w), 1427 (w), 1381 (w), 1341 (w), 957 (m), 859 (s), 816 (m), 730 (s), 666 (m), 621 (s), 488 (w), 456 (w). ^{1}H NMR (400 MHz, D$_2$O): δ 0.92 (m, 42H, CH$_3$), 1.38 (m, 56H, (CH$_2$)$_2$), 1.92 (m, 28H, CH$_2$), 2.37 (s, 12H, CH$_3$), 3.90 (br, 14H, CH), 4.20 (s, 8H, CH$_2$), 7.33, 7.41 ppm (ABq, J = 8.0 Hz, 16H, ArH).

(GlyH)$_9$K$_3$[As$_4$(Mo$^{VI}_3$)Mo$^{VI}_{0.5}$W$^{VI}_{43.5}$Y$_4$O$_{159}$(Gly)$_8$(H$_2$O)$_{11}$]·(Gly)$_6$·15H$_2$O (6). Solid $K_{14}[As_2W_{19}O_{67}(H_2O)]$ (0.5263 g, 0.1000 mmol) was dissolved in 1 M glycine solution (20 mL, 20 mmol) at pH 2.2, with this pH being maintained during the dissolution by addition of concentrated HCl (37%). To this solution was added $Na_2MoO_4{\cdot}2H_2O$ (0.040 g, 0.163 mmol) while the pH was maintained at 2.2 using 3 M HCl. Solid $Y(NO_3)_3{\cdot}6H_2O$ (0.0626 g, 0.163 mmol) was then added, and the pH of the resulting solution was once again adjusted to 2.2. The reaction flask was wrapped in foil and stored in the dark, affording colorless platelike crystals overnight. These were recrystallized (in the dark) by dissolution in a minimum volume of water, followed by dilution with an equivalent volume of 1 M glycine (pH 2.2) to yield a mixture of square and rectangular platelike crystals. Yield: 300 mg, 0.021 mmol (49% based on W). Anal. Calcd (found) for $C_{46}H_{176}N_{23}As_4Mo_{3.5}W_{43.5}Y_4O_{231}K_3$: C, 3.99 (4.2); H, 1.28 (1.4); N, 2.33 (2.4); As, 2.16 (2.2); Y, 2.57 (3.1); Mo 2.42 (2.1); K 0.85 (0.8). Selected IR (KBr, cm^{-1}): 1746(w), 1615 (s), 1481 (m), 1455 (m), 1410 (m), 1336 (w), 1310 (m), 1248 (w), 1108 (w), 951 (m), 862 (s), 800 (m), 717 (s), 616 (s), 489 (w), 460 (w). ^{1}H NMR (400 MHz, D$_2$O): δ 3.70 ppm (CH$_2$).

.

$(GlyH)_6K_{2.5}\{[As_4(Mo^V_2Mo^{VI}W^{VI})Mo^{VI}W^{VI}_{43}Y_4O_{160}(Gly)_8(H_2O)_{12}]_{0.25}[As_4(Mo^{VI}_3W^{VI})Mo^{VI}W^{VI}_{43}Y_4O_{160}(Gly)_8(H_2O)_{12}]_{0.75}\}\cdot(Gly)_{14}\cdot 10H_2O$ (7a). Solid $K_{14}[As_2W_{19}O_{67}(H_2O)]$ (0.5263 g, 0.1000 mmol) was dissolved in 1 M glycine solution (20 mL, 20 mmol) at pH 2.2, with this pH being maintained during the dissolution by addition of concentrated HCl (37%). To this solution was added $Na_2MoO_4\cdot 2H_2O$ (0.040 g, 0.163 mmol) while the pH was maintained at 2.2 using 3 M HCl. Solid $Y(NO_3)_3\cdot 6H_2O$ (0.0626 g, 0.163 mmol) was then added, and the pH of the resulting solution was again adjusted to 2.2 using 3 M HCl. After 10 min, hydrazinium sulfate solution (0.10 M, 400 μL, 0.163 mmol) was added, resulting in deep blue platelike crystals overnight. These were recrystallized by dissolution in the minimum volume of water, followed by dilution with an equivalent volume of 1 M glycine (pH 2.2) to yield a mixture of square and rectangular platelike crystals. Structural analysis of the rectangular platelike crystals by X-ray crystallography afforded the formula $(GlyH)_6K_{2.5}\{[As_4(Mo^V_2Mo^{VI}W^{VI})Mo^{VI}W^{VI}_{43}Y_4O_{160}(Gly)_8(H_2O)_{12}]_{0.25}[As_4(Mo^{VI}_3W^{VI})Mo^{VI}W^{VI}_{43}Y_4O_{160}(Gly)_8(H_2O)_{12}]_{0.75}\}Gly)_{14}\cdot 49H_2O$ (7aw) for the wet crystals. The sample partially dehydrates upon drying. Yield: 500 mg, 0.048 mmol (80% based on W). Anal. Calcd (found) for air-dried 7a, $C_{56}H_{190}N_{28}As_4Mo_4W_{44}Y_4O_{238}K_{2.5}$: C, 4.71 (4.8); H, 1.34 (1.5); N, 2.74 (2.8); As, 2.10 (2.2); Y, 2.49 (2.8); Mo, 2.69 (2.4); K, 0.68 (0.8). Selected IR (KBr, cm^{-1}): 1735 (w), 1621 (s), 1492 (w), 1455 (w), 1429 (w), 1382 (w), 1322 (w), 955 (m), 890 (s), 856 (s), 810 (m), 780 (m), 764 (m), 738 (s), 671 (m), 664 (m), 639 (s), 487 (w), 455 (w), 433 (w). ^{1}H NMR (400 MHz, D_2O): δ 3.70 ppm (CH_2).

$(p\text{-}MeBzNH_3)_2(GlyH)_{7.5}\{[As_4(Mo^V_2Mo^{VI}W^{VI})Mo^{VI}_{1.5}W^{VI}_{42.5}Y_4O_{160}(Gly)_8(H_2O)_{12}]_{0.75}[As_4(Mo^{VI}_3W^{VI})Mo^{VI}_{1.5}W^{VI}_{42.5}Y_4O_{160}(Gly)_8(H_2O)_{12}]_{0.25}\}\cdot(Gly)_{12}\cdot 30H_2O$ (7b). Dis-solution of 4b (67 mg, 0.0046 mmol) in the minimum volume of 1 M glycine (pH 2.2, ca. 1.5 mL) gave crystals of 7b in 70% yield (47 mg, 0.0032 mmol) after 1 day. Structural analysis by X-ray crystallography afforded the formula $(p\text{-}MeBzNH_3)_2(GlyH)_{7.5}\{[As_4(Mo^V_2Mo^{VI}W^{VI})Mo^{VI}_{1.5}W^{VI}_{42.5}Y_4O_{160}(Gly)_8(H_2O)_{12}]_{0.75}[As_4(Mo^{VI}_3W^{VI})Mo^{VI}_{1.5}W^{VI}_{42.5}Y_4O_{160}(Gly)_8(H_2O)_{12}]_{0.25}\}\cdot(Gly)_{13}\cdot 63H_2O$ (7bw) for the wet crystals, which partially dehydrate upon drying. Anal. Calcd (found) for air-dried 7b, $C_{71}H_{253}N_{29.5}As_4Mo_{4.5}W_{43.5}Y_4O_{257}$: C, 5.79 (6.3); H, 1.73 (1.7); 2.81 (2.5); As, 2.04 (1.9); Y, 2.42 (2.4); Mo, 2.93 (2.5); K, 0.00 (<0.5). Selected IR (KBr, cm^{-1}): 1722 (w), 1632 (s), 1479 (w), 1412 (w), 1429 (w), 1384 (w), 1331 (w), 1253 (W), 1120 (W), 954 (m), 864 (s), 800 (m), 779(m), 760(m), 735 (s), 671 (m), 640 (s), 619 (m), 597(m), 513 (m), 490 (w), 455 (w). ^{1}H NMR (400 MHz, D_2O): δ 2.33 (s, 6H, CH_3), 3.70 ppm (s, 56H, CH_2), 4.15 (s, 4H, CH_2), 7.27, 7.36 ppm (ABq, J = 8.4 Hz, 8H, ArH).

X-ray Data Collection and Structure Solution. The crystallo-graphic data (Table S1 in the Supporting Information) for compounds 3w, 4aw, 4bw, 4cw, 7aw, and 7bw (Figure S1 in the Supporting Information) were collected on an Agilent Technologies SuperNova Dual Wavelength single crystal X-ray diffractometer using Cu Kα radiation (λ = 1.5418 Å, mirror monochromated) at 130(2) K. The structures were solved by direct methods (SHELXT) and refined through full-matrix least-squares techniques on F^2 using SHELXL and OLEX2 crystallographic software packages.[60−62] All tungsten, molybdenum, yttrium, and arsenic atoms were refined with anisotropic displacement parameters; all other atoms could only be refined isotopically. The determination of the mixed-metal composition of the polyanions (Figure S2 in the Supporting Information) of 3w, 4aw, 4bw, 4cw, 7aw, and 7bw is described in detail below.

3w. The nominally {M_4} "core" atoms (Figure S2 in the Supporting Information), assigned as Mo, showed anomalously high displacement parameters, suggesting partial occupancy. On refinement, the occupancy factor converged to 0.75, indicating that only three of the four core sites were occupied, the vacant site being equally distributed over four positions, due to the 4-fold symmetry. The occupancy factor was fixed at 0.75 during the rest of the refinement. Some of the metal atoms associated with the {$Y_4M_8L_8$} "ring" and the {AsM_9} lacunary Keggin "triad" (Figure S2), originally assigned as W, also showed anomalously high displacement parameters and partial occupancy on refinement. The chemical analysis indicated 5.5 Mo atoms for each POM, suggesting an excess of Mo (2.5 Mo atoms per POM) over that expected for just the "core" Mo atoms. Accordingly the metal atoms in the moiety associated with the {$Y_4M_8L_8$} "ring" and those metal atoms in the {AsM_9} lacunary Keggin "triad" were interpreted as being a mixture of W and Mo. None of the W atoms in the {AsM_9} lacunary Keggin "belt" (Figure S2) showed significant deviation from full occupancy, and accordingly all were assigned as fully occupied W atoms during the rest of the refinement. The refinement converged with 5.9 Mo per POM (3 Mo in the core, and 2.9 distributed over the rest of the POM replacing W).

4aw. The "core" atom, originally assigned as Mo, showed anomalously small displacement parameters, and on refinement as Mo, the occupancy factor became greater than 1, suggesting that the site was a mixture of Mo and W (0.68:0.32 = 2.7:1.3). As the analysis showed 4.5 Mo per POM, the possibility that the core was composed of only partially occupied W atoms could be discounted, as this would mean that all of the Mo would have to be distributed over the rest of the POM, rather than just 1.8 Mo per POM. As for 3w, above, all metal atoms associated with the {$Y_4M_8L_8$} "ring" and the {AsM_9} lacunary Keggin "triad" showed partial occupancy, when refined as W, and accordingly refinement was continued with these sites being a mixture of W and Mo. Again, none of the W atoms in the {AsM_9} lacunary Keggin "belt" showed significant partial occupancy, and accordingly, all were assigned full occupancy during the rest of the refinement.

4bw, 4cw, 7aw, and 7bw. The refinement of all four structures followed the same procedure for 4aw, giving similar results, except that for 7aw and 7bw there seemed to be no significant substitution of Mo for W in the metal sites of the {AsM_9} lacunary Keggin "triad"; accordingly, these metal atom sites were assigned to be fully occupied W. For 7aw, the OLEX2 "Solvent Mask" procedure was used to remove the contributions of the disordered solvent.

For all six structures, the refinement was carried out with the atoms of the mixed Mo/W sites being constrained to the same position, with the same displacement parameters and with the sum of the occupancy factors at each site being 1. The results from the structural analyses are consistent with the chemical analyses, given that there would be expected to be differences between the composition of a single crystal in comparison to the composition of a bulk sample. The positional disorder of the aliphatic chains of the Nle ligands in 3w, 4aw, 4bw, and 4cw was modeled by restraining the components of the molecules to geometrical estimates. The composition of solvent voids was performed using the Platon software package,[63] on the basis of the chemical analyses of all compounds.

Electrochemistry. Cyclic and steady state rotating disk electrode (RDE) voltammetric experiments were carried out in DMSO with Bu_4NPF_6 (0.05 M) as the supporting electrolyte or in aqueous 0.2 M Gly buffer at pH 2.2. A standard three-electrode cell configuration was employed using a 3 mm diameter glassy-carbon (or glassy-carbon RDE) working electrode and a Pt-wire auxiliary electrode. A Ag/AgCl (3 M NaCl) reference electrode was used in aqueous solutions, while an Ag wire quasi-reference electrode separated from the analyte solution by a sintered-glass frit filled with the electrolyte solution was used in DMSO solution. The potential of the Ag quasi-reference electrode was calibrated against the ferrocene/ferrocenium ($Fc^{0/+}$) couple, and all potentials are reported with respect to this reference scale. Controlled-potential electrolysis was performed in a two-compartment cell equipped with a large-area glassy-carbon plate as the working electrode, a platinum mesh as counter electrode, and the same reference electrode as used in voltammetric experiments. Freshly prepared solutions were used for all electrochemical measurements.

Small-Angle X-ray Scattering (SAXS). Data were collected on a Bruker MicroCalix instrument, using Cu Kα radiation at a wavelength of 1.54 Å. The instrument was run in high flux mode, with the X-ray microsource running at 50 W. Scattered X-rays were detected using a Pilatus 100k detector. Solutions of known concentration were measured in 0.5 or 1.5 mm diameter quartz X-ray capillaries with 10 μm wall thickness (Hilgenberg, Germany). Scattering and transmission measurements were made for each of the samples, as well as for a sample containing only the blank solution. Scattering patterns were

collected for 180 min and transmission measurements for 5 s. Initial data processing (normalization, primary beam masking, and background subtraction) was carried out in fit-2D. No smoothing was used, and the data quality was not significantly affected by normalization. Scattering curves were recorded in the range 0.06−0.6 $Å^{-1}$. A low q (0.06−0.17 $Å^{-1}$) Guinier analysis was carried out using ATSAS 2.7.0, yielding an independent measure of the radius of gyration (R_g) and forward scattering (I_0). For comparison to the solution experimental data, the SolX computer program was used to calculate theoretical scattering patterns and R_g values using single-crystal X-ray diffraction data as input.[64,65] Pair distance distribution functions (PDDFs) were obtained from fits to the I(q) data using the inverse Fourier transform (FT) method of Moore[66] as implemented in the Irena software package for Igor Pro.

Other Measurements. Infrared spectra (KBr disk) were recorded on a Bruker Tensor 27 FTIR spectrometer. X-ray photoelectron (XPS) spectra were recorded on a Thermo Scientific K-Alpha Photoelectron Spectrometer system with a monochromated, micro-focused Al Kα X-ray source. Calibration of all spectra was attained by reference to the carbon 1s signal with a binding energy of 285.0 eV. A small degree of X-ray-induced photoreduction was observed during data acquisition, with the Mo^V/Mo^{VI} ratio gradually increasing over many scans for all compounds, especially the oxidized species 3 and 6. All elemental analyses were performed at the Campbell Micro-analytical Laboratory, University of Otago; the CHN analyses employed a Carlo Erba EA 1108 Elemental Analyzer, while ICP-MS analyses for As, K, Mo, and Y employed an Agilent Technologies 7500ce quadrupole ICP-MS instrument. Electronic absorption was measured on an Agilent Technology Cary60 UV−visible spectrometer, and reflectance spectra were measured on a Thermo Scientific-Evolution 220 UV−visible spectrometer. Circular dichroism (CD) spectra were measured on an Aviv Model 410SF spectrometer, and spectra were obtained by averaging eight spectra with a scanning speed of 30 nm min^{-1}. ^1H NMR spectra were acquired on a Varian MR400 400 MHz spectrometer and referenced to residual HDO. $^{13}C\{^1H\}$ and $^1H-^{13}C$ NMR spectra were acquired on a Bruker Avance-II-800 MHz spectrometer and referenced to MeOH.[67]

Computational Details. Density functional theory (DFT) calculations were carried out on structures based on the title compounds. The computed structures include the full inorganic part of the polyanions, whereas the amino acid ligands are replaced by formate groups. This simplification considerably reduces the computational time without affecting the quality of the results of interest or the conclusions provided by the quantum chemical analysis. We used the ADF2013.01 suite of programs[68] to get optimized geometries and molecular energies applying the BP86 functional and to draw 3D representations of the molecular orbitals.[69] The valence electrons of all atoms were described by triple-ζ + polarization (TZP) Slater-type basis sets, with a total of ~7000 Cartesian basis functions per molecule. Internal or core electrons (C, O, 1s; As, 1s−3d; Mo, 1s−4p; W, 1s−4f; Y, 1s−4p) were kept frozen, each described by a single Slater function (1870 in total) with core potentials generated using the DIRAC program.[68a] Scalar relativistic corrections were included by means of the zeroth-order regular approximation (ZORA) and solvent effects of water (characterized by the dielectric constant ε = 78.4) with the conductor-like screening model (COSMO[70]) at every SCF cycle of the computation.

RESULTS AND DISCUSSION

Syntheses. The general procedure for the synthesis of the $[As_4(M_4)Mo^{VI}_xW^{VI}_{44-x}Y_4O_{160}(AA)_y(H_2O)_z]^{n-}$ family involves dissolution of $K_{14}[As_2W_{19}O_{67}(H_2O)]$ in a solution of the appropriate amino acid with maintenence of the pH at 2.2. Sodium molybdate is added for the Mo-containing analogues, followed by yttrium nitrate, affording a clear solution. In the presence of Mo, the solution immediately begins to turn blue due to photoreduction by ambient light. The previously reported synthesis of norleucine compound 2 involves exposure to a UV lamp overnight to generate a photoreduced solution, with norleucine being the likely electron donor. Addition of p-$MeBzNH_3^+$ cations to the blue solution yields 2 as a crystalline product. We have subsequently rationalized that the nature of compound 2 as a mixture of POMs in two redox states, the fully oxidized homovalent M^{VI} (M = Mo, W) species and the 2e-reduced $\{Mo^V_2\}$-containing analogue, probably results from the fact that the compound begins to crystallize from solution before all polyanions are reduced. In an effort to overcome this and access our initial target of a fully 2e-reduced $\{Mo^V_2\}$-containing POM, we turned to chemical reduction rather than photoreduction, selecting hydrazinium sulfate as a convenient reductant because of its reasonable stability and successful employment in the synthesis of other reduced POMs.[21] In addition to varying the amount of hydrazinium, we also varied the amount of added molybdate in a targeted effort to obtain the tetrasubstituted 2e-reduced $[As_4(Mo^V_2Mo^{VI}_2)W_{44}Y_4O_{160}(AA)_x(H_2O)_y]^{n-}$ analogue, rather than species with mixed metals in the central tetranuclear core. This target theoretically requires 1.74 mol equiv of molybdate and 0.22 mol equiv of hydrazinium per $[As_2W_{19}O_{67}(H_2O)]^{14-}$, given that hydrazinium is formally a 4e reductant and assuming complete conversion of the POM precursor to the hybrid POM product. However, multiple equilibria appear to be involved in the formation of the hybrid POM in solution, and we found that the use of stoichiometric molybdate in fact affords products with more than four Mo centers per POM (see later) and that, for a given amount of molybdate, variation of the amount of hydrazinium controls the extent of incorporation of Mo. Ultimately we settled on 1.6 mol equiv of Mo and 0.22, 0.44, and 0.87 mol equiv of hydrazinium to explore norleucine analogues with 4.5 (4a), 5 (4b), and 5.5 (4c) Mo atoms per hybrid POM, respectively. These compounds are obtained in moderate yields as homogeneous crystalline samples of tetrahedral-shaped crystals (Figure S1 in the Supporting Information). Redissolution and ^1H NMR spectroscopy indicate that all samples are diamagnetic. Even when a four-fold excess of hydrazinium is used, coulometry suggests that the products are 1.8(2) electrons reduced (see later), apparently always a little short of the target 2e reduced, although for simplicity, 4a−c are formulated herein as comprised of only the 2e-reduced $\{Mo^V_2\}$-containing analogue. The use of more hydrazinium in attempts to access a further reduced species affords a green-blue solution from which crystals could not be obtained. Synthesis of the racemic DL-norleucine-containing analogue 5 was performed using the same amounts of molybdate and hydrazinium as 4b, affording crystals of a morphology different from that of 4b, which were unsuitable for single-crystal X-ray diffraction. The infrared and electronic absorption spectra of 5 (see later) suggest that it is overall less reduced than 4b; coulometric oxidation (see later) gives a value of approximately 1.3(2) electrons per POM, and ^1H NMR indicates that the sample is diamagnetic. These data are interpreted as a sample comprised of a mixture of two hybrid polyanions with different redox states: the fully oxidized homovalent M^{VI} (M = Mo, W) species and the 2e-reduced $\{Mo^V_2\}$-containing analogue. For simplicity, 5 is formulated as comprised of an equal mixture of oxidized and 2e-reduced hybrid POMs.

The synthesis of the reduced glycine-containing analogue 7a essentially parallels that of the norleucine-containing analogues, although a higher concentration of glycine is required, as the use of a lower concentration of glycine instead gives rise to an

analogue of a previously reported different compound.[58] The amount of hydrazinium again affects the extent of Mo substitution, with 7a obtained from the same ratio of molybdate to hydrazinium to $K_{14}[As_2W_{19}O_{67}(H_2O)]$ as employed for 4b. In the case of 7a, recrystallization of the crude product is required to generate crystals suitable for single-crystal X-ray diffraction, affording a mixture of rectangular and square platelike crystals. Samples of 7a for all studies reported herein were similarly recrystallized. The degree of reduction of 7a was determined by coulometry as approximately 0.7(2) electron per POM and is consistent with the extinction coefficients determined from electronic absorption spectroscopy (see later). Compound 7a is also diamagnetic and is thus formulated as a 3:1 mixture of oxidized and 2e-reduced hybrid POMs.

Circular dichrosim experiments (see later) suggested the possibility of exchanging glycine and norleucine ligands, and subsequently Gly-containing 7b was obtained in good yield by recrystallizing Nle-containing 4b from 1 M glycine. Compound 7b is significantly darker in color than 7a, indicating that it has a higher proportion of the 2e-reduced POM. The degree of reduction of 7b was determined by coulometry as approx-imately 1.5(2) electrons per POM and is consistent with the extinction coefficients determined from electronic absorption spectroscopy (see later). The lesser degree of reduction found for 7b than for the parent 4b suggests that partial oxidation has accompanied the recrystallization step. ^{1}H NMR spectroscopy of 7b confirms complete exchange of the norleucine ligands for glycine. Compound 7b is thus formulated as a 1:3 mixture of oxidized and 2e-reduced hybrid POMs.

The possibility of isolating samples comprised of only the oxidized Mo^{VI}-containing hybrid POM became apparent during the explorations of the synthesis if the reduced analogues. Both Nle- and Gly-containing analogues 3 and 6 were synthesized without addition of a reductant, with the early addition of p-$MeBzNH_3^+$ cations key in the case of 3. In both cases, the reaction and, in the case of 6, recrystallization solutions were covered by aluminum foil and kept in the dark to avoid photoreduction, although the top of the flask was not sealed to allow a certain degree of evaporation. Solutions of both 3 and 6 are susceptible to photoreduction by ambient light, although 6 photoreduces significantly more rapidly than 3. The crystals (Figure S1 in the Supporting Information) of 2, 3, and 4a−c all exhibit a tetrahedral morphology, while 6 and 7a,b are comprised of a mixture of square and rectangular platelike crystals. However, while the reduced species 2, 4, 5, and 7b are deep blue in color and 7a is medium blue, the crystals of oxidized 3 and 6 exhibit a very faint blue tint, which is likely due to a small degree of photoreduction on the crystal surface.

Solid State Studies. Composition Determination and General Comments. Bulk samples of the compounds are crystalline and homogeneous to the eye, and all were characterized by elemental analysis and IR and XPS spectroscopy. A single crystal type was evident in all of the Nle-containing compunds, while two crystal types were present in the Gly-containing compounds 6 and 7a,b, only one of which was amenable to characterization by single-crystal X-ray diffraction. Wherever possible, single-crystal diffraction data were collected for multiple crystals from different batches to test reproducibility from batch to batch and also homogeneity within a batch. The single-crystal data were generally in agreement with the bulk analytical data, with crystal to crystal variations of less than 10% in the site-specific Mo/W occupancy values (see later). Metal analyses indicated 5.5, 4.5, 5, 5.5, and 3 Mo centers per hybrid POM for norleucine-containing 3, 4a−c, and 5, respectively (Table S2). Glycine-containing 6 and 7a,b analyzed for 3.5, 4, and 4.5 Mo centers per molecule. The single-crystal data reported herein are for individual crystals of 3w, 4aw−cw, and 7aw,bw with respectively 5.9, 4.6, 5, 5.5, 4.6, and 4.8 Mo atoms per hybrid POM (Table S2 in the Supporting Information). The formulations given for all compounds reflect the average composition of the bulk samples on the basis of the elemental analysis and ^{1}H NMR spectra, combined with the degree of reduction determined from electrochemical and spectroscopic data (see later). As reported previously, magnetic susceptibility and EPR measurements performed on solid samples of the reduced compounds indicate that they are diamagnetic, consistent with the solution ^{1}H NMR spectroscopy.

Structural Analysis. Single-crystal X-ray diffraction data (Table S1 in the Supporting Information) indicate that Nle-containing compounds 3w and 4aw−cw are isomorphous with the previously reported compound 2, crystallizing in the enantiomorphic cubic space group $F432$. The rectangular platelike crystals of the Gly-containing compounds 6 and 7aw,bw are isomorphous and crystallize in the monoclinic space group $P2_1/n$; although a high-quality data set could be obtained for these crystals of 7, this was not possible for 6. The square platelike crystals of 6 and 7aw,bw were very poorly diffracting, although in all three cases they appear to be isomorphous and belong to the triclinic space group $P\bar{1}$ with similar unit cells (a = 16.800(3) Å, b = 28.740(6) Å, c = 30.070(3) Å; α = 83.00(3)°, β = 77.54(3)°, γ = 77.90(3)°).
The structure of the hybrid POMs in each compound are based on the $[As_4(M_4)Mo^{VI}_xW^{VI}_{44-x}Y_4O_{160}(AA)_y(H_2O)_z]^{n-}$ (M = Mo/W) generic unit, with four trilacunary α-Keggin $\{AsM_9\}$ moieties linked by a $\{Y_4M_8L_8\}$ "ring" fragment (L = zwitterionic Gly, 6 and 7; L = L-Nle, 3 and 4) with an inner oxo-bridged "core" (Figure 2 and Figure S2 in the Supporting Information). Two types of zwitterionic amino acid ligands bridge pairs of W centers or pairs of Y centers via carboxylate groups (Figure S3 in the Supporting Information), with the protonated amine groups involved in intramolecular hydrogen bonding to the $\{AsM_9\}$ fragments with N(−H)···O distances of 2.8−3.0 Å. The $\{M_4\}$ core metal centers have trans oxo-aqua terminal ligands, with a ninth monodentate norleucine ligand disordered with these aqua ligands in 4aw−cw (Figure S3).

An intriguing difference is that while compounds 2, 4aw−cw, and 7aw,bw exhibit the expected $\{M_4\}$ core (M = disordered Mo and W), the oxidized homovalent M^{VI} (M = Mo, W) analogue 3w possesses a monovacant $\{Mo_3\}$ core (Figure 2), with 75% Mo occupancy for each of the four sites and no tungsten. This difference in the central core is despite the isomorphous structures of 2, 3, and 4aw−cw. Although a high-quality X-ray data set could not be obtained for 6, it is formulated herein with a trimetallic core by analogy with the other fully oxidized species, 3, and this formulation is supported by the similarity of the IR spectra of the two compounds (see later) in comparison to the spectra of the reduced analogues, as well as DFT calculations (see later). However, this formulation requires better crystallographic data to be definitive.

Close inspection of the single-crystal X-ray diffraction data of all analogues reveals disorder of Mo/W in many of the metal positions, with the site occupancies summarized in Table S2 in the Supporting Information. Incorporation of Mo into the metal positions shows considerable selectivity, with the Mo site occupancy decreasing in the same order for all analogues: $\{M_4\}$

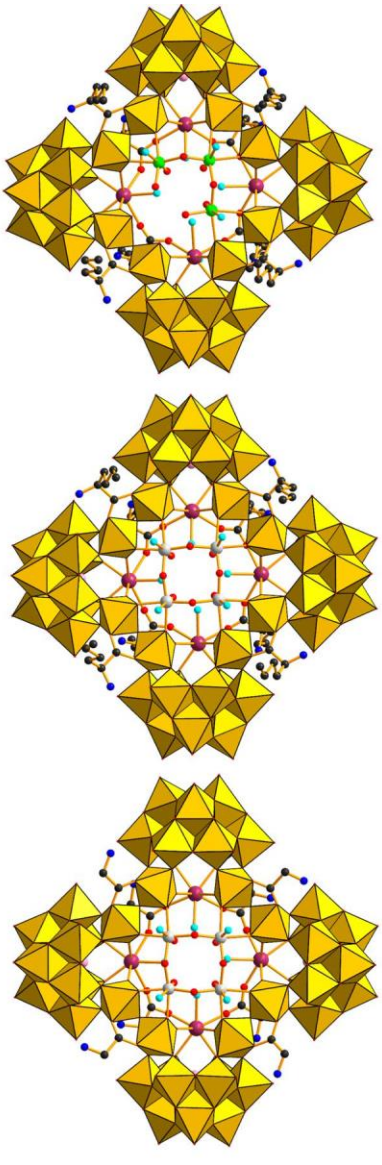

Figure 2. Structural representations of the molecular structures of (top) 3, (middle) 4b, and (bottom) 7a. Color code as per Figure 1 with Mo given in green.

or {M_3} core > {$Y_4M_8L_8$} "ring" > {AsM_9} "triad" > {AsM_9} "belt" (Figure S2 in the Supporting Information). A significant preference for the inner {M_4} or {M_3} core is evident with between 68 and 88% Mo occupancy. In no case is any Mo evident in the "belt" positions of the {AsM_9} units. These occupancies can be interpreted in terms of the likely disassembly/reassembly from the $[As_2W_{19}O_{67}(H_2O)]^{14-}$ precursor, with the smallest extent of Mo for W exchange during complex formation occurring in the trilacunary α-Keggin {AsW_9} fragments that are present in the POM precursor.

Bond valence sum (BVS) calculations are challenging for species with mixed-metal site occupancies,[71] especially for those that are also mixed valence; with this caveat in mind the BVS values for the cores of compounds 4aw−cw and 7aw,bw are consistent with oxidation states between penta- and hexavalent, while the other W/Mo positions are hexavalent for all compounds. Bond valence sum calculations on all bridging oxo ligands for all compounds give values in the range 1.7−2.2, consistent with an absence of localized protonation to hydroxo ligands.[72] It must be noted that while reduced compounds 4a−c are formulated with 2e-reduced $\{Mo^{V}_2Mo^{VI}W^{VI}\}$ cores, it is impossible to experimentally distinguish between this situation and the same equal mix of compounds with 2e-reduced $\{Mo^{V}_2Mo^{VI}_2\}$ and $\{Mo^{V}_2W^{VI}_2\}$ cores. Spectroscopic and electrochemical data (see later) indicate that compounds 5 and 7a,b are mixtures of different proportions of fully oxidized homovalent M^{VI} (M = Mo, W) and 2e-reduced $\{Mo^{V}_2\}$-containing complexes; all compounds are diamagnetic. It is notable that single-crystal X-ray diffraction data for all photoreduced and/or chemically reduced mixed Mo/W analogues of this family of compounds exhibit full occupancy of the tetranuclear core, indicating there is no component with a trinuclear core as is observed for oxidized species 3.[54,73] Given no evidence for a component with a trinuclear core and core Mo occupancies in the range 68−88%, "partially reduced" compounds 5 and 7a,b are formulated as mixtures of complexes with hexavalent $\{Mo^{VI}_3W^{VI}\}$ and 2e-reduced mixed-valent $\{Mo^{V}_2Mo^{VI}W^{VI}\}$ tetrametallic cores.

Comparison of the diffraction data for compounds 3w, 4aw−cw and 7aw,bw provides insight into the effects on the POM molecular structure of (i) different degrees of reduction, (ii) tri- versus tetrametallic core, and (iii) norleucine versus glycine ligands. In all compounds the outer framework comprised of four trilacunary α-Keggin {AsM_9} moieties linked by the cyclic {$Y_4M_8L_8$} fragment is conserved, with little structural variation and essentially no dependence on the nature of the amino acid ligand, the nuclearity of the inner core, or the variation in Mo/ W occupancies. The more flexible part of the structure is the central core, and it is intriguing that while a tetrametallic core is obtained for all reduced species, in the absence of reduction a trimetallic {Mo_3} core is obtained in the case of Nle-containing 3w and a highly distorted {W_3Y} is evident for previously reported fully oxidized Gly-containing 1. It is curious that a homotetrametallic {Mo_4} or {W_4} compound is yet to be definitively characterized for any analogue of this structural family. This may reflect the specific size and binding characteristics of this structural pocket and subtle differences in ionic radii between M^{VI} and M^{V} (M = Mo, W). The most notable structural differences between the trimetallic fully oxidized core of 3w and the tetrametallic reduced cores of 4aw−cw are the shorter M···M separations and more acute M− O−M angles for 3w (Table S2 in the Supporting Information), reflecting an overall smaller central core in this compound.

As was observed previously for 1 and 2, the Nle- and Gly-containing analogues differ in the arrangement of the amino acid ligands (Figure S4 in the Supporting Information). For isomorphs 2, 3w, and 4aw−cw the four Nle ligands that bridge W centers rotate in the opposite sense to the four that bridge Y centers. In contrast, for 1 and 7aw,bw all eight Gly ligands are oriented in the same direction. This is despite the fact that compounds 1 and 7aw/7bw exhibit different crystal packing, with 1 incorporating p-$MeBzNH_3^+$ ligands that are absent in 7aw/7bw. The arrangement of the ligands in the Nle-containing compounds likely reflects both the necessity of accommodating relatively hydrophobic n-butyl chains and the different crystal packing.

The isomorphous Nle-containing compounds 2, 3w, and 4aw−cw crystallize in the chiral space group F432, with each crystal comprised of one enantiomeric form of the polyanion. The polyanions pack such that they occupy the six faces of approximately cubic-shaped cavities, which are lined by the n-butyl chains of Nle ligands (Figure S5 in the Supporting

Information). The differing "top" and "bottom" faces of the disklike polyanions give rise to two types of these cavities. The contents of both of these cavities, as well as the channels that run in all three directions, are crystallographically disordered. Approximate void calculations using the Platon software package[63] result in total void volumes consistent with the accommodation of the cations, free amino acid, and water molecules of hydration given in the formulations of 3w and 4aw−cw. The closest intermolecular W···W separation in Nle-containing compounds is 6.1 Å. In contrast to the Nle-based analogues, the polyanions in the Gly-containing compound 7aw,7bw pack in offset alternating double layers (Figure S6 in the Supporting Information). The closest intermolecular W···W separation is 5.9 Å, and there are no intermolecular hydrogen-bonding interactions between polyanions. Again the cations, free glycine, and hydrate molecules are disordered and the calculated total void volume is consistent with the formulations given for 7aw,bw.

Infrared Spectroscopy. Infrared spectra were acquired for compounds 3, 4a−c, 5, 6, and 7a,b as pressed KBr disks. All spectra exhibit bands consistent with the presence of the amino acid ligands and organic cations (Figure S7 in the Supporting Information). Comparison of the fingerprint region below 1100 cm^{-1} is informative (Figure S8 in the Supporting Information), as this region is dominated by the intense bands of the POM backbone. The spectra for oxidized compounds 3 and 6 are very similar, with five broad bands in the region 550−1000 cm^{-1}. Four of these bands between 650 and 1000 cm^{-1} strongly resemble the spectrum of the $K_{14}[As_2W_{19}O_{67}(H_2O)]$ precursor and are assigned as follows: the band at ~950 cm^{-1} is attributed to the terminal M O (M = Mo, W) stretch, the broad band at 860 cm^{-1} with a shoulder at 900 cm^{-1} is due to the corner-sharing M−O−M stretches, and the two bands at 720 and 800 cm^{-1} are due to edge-sharing M−O−M stretches, possibly overlapping with the As−O−M stretches.[74] The strong similarity between the spectra of 3 and 6 supports the proposition that the trimetallic core that is crystallographically observed for 3 is likely also present in 6. Upon reduction, spectral changes are evident for analogues 4, 5, and 7 with a tetrametallic core. Between 820 and 1000 cm^{-1} the spectra resemble those of the oxidized species, with the addition of a shoulder at around 970 cm^{-1}. Below 820 cm^{-1}, the three bands evident for 3 and 6 appear to be split, broadened, and shifted for the reduced analogues 4, 5, and 7. Shifting of M−O−M stretching bands and spectral broadening upon reduction have been observed previously for several POMs, with the extent of broadening dependent on the degree and site of localization/delocalization of the reducing electrons.[75−79] The subtle difference among the spectra for 4a−c presumably arise from the small differences in Mo content. It is notable that the spectrum of 5 appears intermediate between those of oxidized 3 and 2e-reduced 4, consistent with a mixture of the two oxidation states. The spectra of 7a,b both appear to combine some of the features of 3 and 6 with the increased spectral complexity in the 550−700 cm^{-1} range that is evident for 4 and 5. The spectra are qualitatively consistent with 7a,b both being comprised of a mixture of oxidized and 2e-reduced hybrid POMs, with a higher proportion of oxidized POM in 7a than in 7b.

X-ray Photoelectron Spectroscopy (XPS). X-ray photoelectron spectra were measured for representative oxidized compounds 3 and 6 and reduced compounds 4b and 7a. The W 4f and Mo 3d spectra are available in Figure S9 in the Supporting Information, and the binding energies from spectral deconvolution are given in Table S3 in the Supporting Information. Literature binding energies for the W $4f_{7/2}$ and $4f_{5/2}$ peaks average around 35.5 and 37.9 eV for W^{VI} and 34.1 and 36.7 eV for W^{V}.[80,81] The W 4f spectra for 3, 6, 4b, and 7a all exhibit only the doublet associated with W^{VI} at binding energies of 35.8−36.6 and 37.9−38.7 eV, with no indication of any W^{V} or W^{IV} in any of the compounds. The signal to noise is much poorer for the molybdenum spectra, due to the relatively small amounts of Mo in each of the compounds. Literature binding energies for the Mo $3d_{5/2}$ and $3d_{3/2}$ peaks average around 232.7 and 235.9 eV for Mo^{VI}, 231.5 and 234.2 eV for Mo^{V}, and 229.5 and 233.0 eV for Mo^{IV}.[49,80,82,83] We have previously found that the Mo-containing analogue 2 was photoreduced during XPS measurements, with the reduction taking place at the Mo sites and apparent in the Mo spectra. Similar photoreduction was observed for the present compounds, with all compounds exhibiting spectra that can be deconvoluted to give components characteristic of Mo^{VI} and Mo^{V}, with Mo^{VI} doublets in the ranges 232.4−233.3 and 236.0−236.5 eV and Mo^{V} doublets in the range 231.2−233.1 and 234.1−235.6 eV. The amount of Mo^{V} increases at the expense of Mo^{VI} as the number of scans increases. Confining our analysis to the minimum number of scans required for reasonable signal to noise, we can semiquantitatively confirm that reduced compounds 4b and 7a have more Mo^{V} than do oxidized compounds 3 and 6. The tungsten and molybdenum XPS spectra definitively confirm that reduction takes place site selectively at molybdenum rather than tungsten centers.

Solution Studies. Determination of Solution Structure and Stability. Determination of the degree (and site) of reduction of the reduced hybrid POMs in this study is essential to establish their chemical formulas. Measuring the degree of reduction is best achieved by coulometry; however, for the results of electrochemical studies to be meaningful, it is first necessary to establish the stability of the hybrid POM in solution. In the present study, multiple physical techniques were employed for this purpose. In the first instance, electronic absorption spectroscopy of the reduced compounds provides a simple probe for monitoring changes in the degree of reduction over time. Small angle X-ray scattering allows establishment of the size and shape of the metal−oxo POM framework. Circular dichroism and ^1H NMR spectroscopy provide information on the amino acid ligands of the hybrid POMs.

The solubility properties of the different analogues depend on the amino acid, degree of reduction, and overall charge. In our initial exploration of solution properties we opted to redissolve the compounds in aqueous solution at pH 2.2−2.4, which is the pH at which the compounds crystallize. In all cases, dissolution of the hybrid POMs is much more facile in the presence of an excess of the amino acid ligand. Thus, the solution studies discussed below have employed a buffer of the corresponding amino acid, in addition to water acidified with HCl. As DMSO proved to be the solvent of choice for voltammetric characterization of the reduced Nle-containing compounds (see later), we also measured solution properties in DMSO for the Nle analogues only, as the Gly analogues are insoluble. Instability of the reduced POMs in solution is readily apparent from rapid loss of the blue color, which occurs when the pH of the solution is taken outside the range of around 1.5−4.0. Solutions within this pH range with a POM concentration of greater than 0.2 mM appear to be stable on

the order of days, although decomposition and/or further aggregation is apparent after 1 week in most cases (see later).

Electronic Absorption Spectroscopy. To investigate solution stability in the presence and absence of excess amino acid, electronic absorption spectra in the visible range (Figure 3 and

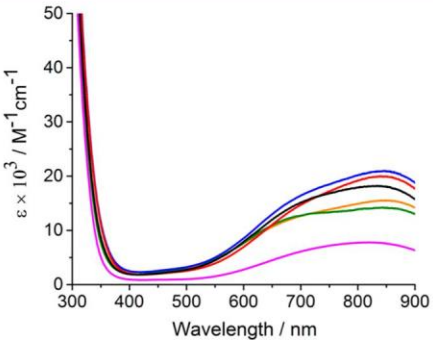

Figure 3. Electronic absorption spectra of 0.028 mM solutions of 4a (black), 4b (red), 4c (blue), 5 (green), 7a (pink), and 7b (orange) in 0.15 or 0.2 M corresponding amino acid buffer (pH 2.2).

Figures S10−S12 and Table S4 in the Supporting Information) were measured for the blue $\{Mo^{V}_{2}\}$-containing reduced compounds 4a−c, 5, and 7a,b (0.028 mM) in the corresponding amino acid buffer (0.15 Nle or 0.2 M Gly, pH 2.2) and aqueous solution in the absence of excess amino acid (pH adjusted to 2.4 with 3 M HCl prior to dissolution and checked after dissolution). Absorption spectra were also measured in DMSO for the Nle analogues.

The electronic absorption spectra for 4a−c, 5, and 7a,b in buffered and unbuffered aqueous solution and in DMSO all exhibit the strong oxo to metal LMCT bands typical of POMs in the UV region. The visible region in all spectra is dominated by at least two overlapping broad bands between 600 and 900 nm, consistent with the blue coloration, in addition to much weaker bands between 400 and 500 nm. The bands between 600 and 900 nm can be assigned to $Mo^{V} \rightarrow M^{VI}$ (M = Mo, W) IVCT bands that are typical for Mo blues and reduced POMs generally, while Mo^{V} d−d transitions are likely responsible for the weaker bands between 400 and 500 nm.[20,75,84−86] The particular characteristics appear to vary with (i) the solvent medium, (ii) the degree of reduction, and (iii) the degree of Mo for W substitution (Figure 3 and Figures S7 and S8 in the Supporting Information). Notably for all compounds, spectra measured in aqueous solution without excess amino acid are less intense than those obtained in either buffer or DMSO (Figure S7). The origin of this difference in extinction coefficients is not clear, but the observation points to a decreased stability in the absence of excess amino acid, which is more pronounced for the norleucine analogues than for the glycine species. For the norleucine compounds, the spectra for 5 are all indicative of a lower overall degree of reduction than for 4a−c, which is consistent with results from electrochemical studies (see later). It is interesting to compare the spectra measured for 4a−c, which although of similar degree of reduction vary in the relative amounts of Mo and W. In buffer, DMSO, and water the spectra of compounds 4a−c possess two distinct band maxima at ca. 850 and 700 nm, which can be tentatively assigned to $Mo^{V} \rightarrow Mo^{VI}$ and $Mo^{V} \rightarrow W^{VI}$ IVCT transitions, respectively, on the basis of literature studies of mixed-valence mixed Mo/W POMs.[75,84−86] In all solvents, the relative intensities of these two bands are closer for 4a, while for 4b,c, the lower energy band is more intense, which might reflect the increase in Mo content from 4a to 4b and 4c. Regardless of the media, the relative intensities of the spectra measured for the different compounds (4b,c > 7b > 5 > 7a) are consistent with the overall decrease in the degree of reduction determined by coulometry (see later), which corresponds to the proportion of 2e-reduced $\{Mo^{V}_{2}\}$-containing versus homovalent M^{VI} (M = Mo, W) POM in each compound.

Changes in the absorption spectra over time were investigated for all solutions and found to be strongly dependent on the POM concentration (Figure S12 in the Supporting Information). It was found that, as long as the POM concentration is greater than about 0.15 mM and the pH is in the 2.2−2.4 range, the spectra exhibit little change in aqueous buffer solution and in DMSO on a time scale of hours, which is sufficient for the CD, SAXS, and electrochemical measurements discussed below. More dilute solutions appear to undergo either oxidation or decomposition of the polyanion.

Small-Angle X-ray Scattering (SAXS). Representative oxidized and reduced Nle and Gly analogues 3, 4b, and 7a were investigated in solution by SAXS to probe the stability of the hybrid POM under different conditions, as well as the sensitivity of the technique to the presence of the aliphatic n-butyl chain on the amino acid ligands. The effect of varying both the POM (0.2−1.2 mM) and amino acid buffer (0.1−1.0 M, pH 2.2) concentration was also explored, as was the effect of pH variation (pH 0.15−4.0) in unbuffered HCl solution. Samples were measured immediately following dissolution, and the data collection time was in the range of 3−9 h.

The scattering plots of intensity ($I(q)$) versus the scattering vector (q), measured for 3, 4b, and 7a in amino acid buffer and in unbuffered HCl at pH 2.2, are in reasonable agreement with plots calculated by inputting the solid-state single-crystal X-ray diffraction data into the SolX program (Figure 4).[64,65] Good linear fits are obtained in the Guinier regime (q = 0.06−0.17 $Å^{-1}$) for POM concentrations of 0.7 mM or less (Figure S13 in the Supporting Information), while some interaction effects are evident for higher concentrations. The radius of gyration (R_g) is a shape-independent measure of the size of the hybrid POM molecules in solution, and R_g values obtained from the Guinier fits are given in Table S5 in the Supporting Information. The R_g values determined for the three different analogues in amino acid buffer are in the range 8.2(4)−9.4(4) Å, in excellent agreement with the values of 8.3−8.6 Å calculated from single-crystal data. The scattering plots and R_g values are consistent with maintenance of the solid-state structure in solution and show that the solution is monodisperse: i.e., only polyanions of a single size are present. Variation of the hybrid POM concentration (0.2−1.2 mM), the buffer concentration (0.10− 0.15 M), and pH (1.5−4.0) for 4b has little effect on the scattering plots or R_g values (Table S5), indicating the general stability of the hybrid POM of 4b under these defined conditions. However, the SAXS technique is apparently insensitive to the length of the aliphatic chain on the amino acid ligand, with no significant difference between the scattering plots and R_g values measured for 4b and 7. This is most likely due to minimal electron density contrast between the organic ligands and the solvent.

To complement the Guinier plots, which provide a shape-independent measure of the average size, the radial pair distance distribution functions (PDDFs) were determined for all solutions to provide information about the shape of the hybrid POM (Figures S14 and S15 in the Supporting

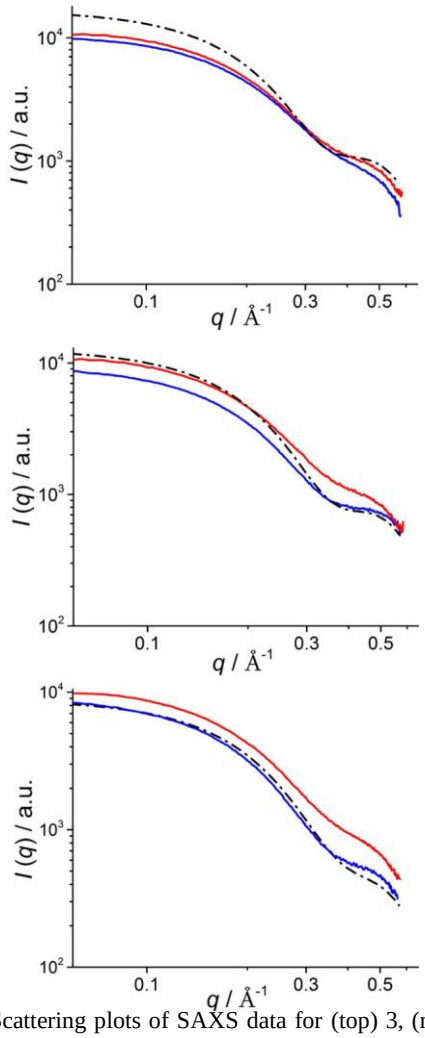

Figure 4. Scattering plots of SAXS data for (top) 3, (middle) 4b, and (bottom) 7a (0.7 mM polyanion) in 0.15 M L-NLe or 0.2 M glycine buffer at pH 2.2 (blue) and unbuffered HCl at pH 2.2 (red). The dashed lines are the curves calculated from the single-crystal diffraction data (SolX, normalized to experimental data in buffer).

Information). The PDDF is the probability, P(r), that a component of the particle is at a distance, r, from the edge of the particle (r = 0). These were calculated using Moore's method[66] and compared with PDDF curves calculated from the single-crystal X-ray diffraction data. In general, reasonable agreement is evident between the measured SAXS data and the plots calculated from the solid-state structure for the aqueous solutions of 3, 4b, and 7a. Notably, the point at which P(r) goes to zero is in the range 27−33 Å and is consistent with the crystallographically determined diameters of the hybrid POMs. The curves all exhibit two maxima and in most cases a minor feature at large r, clearly indicating that the hybrid POMs are not spherical. The profile is consistent with the overall shape of the molecules, which all have a low-density region in the central core, corresponding to the minimum between the two main peaks i.e. the probability of finding an atom in the center of the hybrid POM is lower than that elsewhere. There are subtle differences in the relative heights of the maxima between the SAXS and crystal data. This could be related to particle flexibility in solution in comparison to that in the crystal, as well as the variation in electron density contrast between the solvent and regions of the POM structures under different solution conditions. The R_g values obtained from the PDDF plots (Table S5 in the Supporting Information) are in excellent agreement with the values from the Guinier plots.

Compounds 3 and 4b were also measured in DMSO (Figure S15 in the Supporting Information), as this was the solvent of choice for electrochemistry (see later). Although the scattering intensity is markedly less than in aqueous solution due to the strong X-ray absorption of DMSO, the scattering plot and PDDF measured for 4b are in reasonable agreement with the calculated curves. While the poor signal to noise at high q impaired the accuracy of the PDDF fitting procedure, the Guinier fit was unaffected, and the R_g values obtained are consistent with the values obtained in aqueous media (Table S5 in the Supporting Information). This suggests that the hybrid POM of 4b is stable in DMSO on the time scale of the SAXS measurement. By comparison, the scattering curve measured for 3 is in poor agreement with the calculated curve, and the value of R_g determined for 3 in DMSO is significantly smaller than those obtained in aqueous solutions or from simulation. Thus, the oxidized hybrid POM of 3 appears to be unstable in DMSO on the time scale of the SAXS measurement.

On a longer time scale, measurements of 3 and 4b in buffered and unbuffered aqueous media 1 week after dissolution reveal changes in the R_g values in all cases. Interestingly, while the R_g values decrease in the absence of norleucine buffer, they increase in the presence of buffer, by 10−20%. The change evident for 3 is greater than for 4b in both cases. These changes on the longer time scale of a week point to decomposition in the absence of excess Nle but aggregation in the presence of excess norleucine. The latter case perhaps corresponds to the formation of the well-known POM "blackberries" or "vesicles".[87]

Circular Dichrosim (CD) Spectroscopy. Small-angle X-ray scattering established the maintenance of the metal−oxo POM framework in buffered solution for the reduced Gly and Nle analogues but provides no information on whether the amino acid ligands remain coordinated. The presence of electronic transitions in the visible region, and the accessibility of enantiomeric and racemic versions of the reduced Nle analogues, prompted the use of CD spectroscopy to investigate solution chirality and ligand exchange for some of the (blue) reduced analogues of the present hybrid POMs. A similar CD-based approach allowed the elucidation of the kinetics of ligand exchange of enantiopure thiolate ligands with gold nano-particles.[88] Spectra were acquired for representative compounds 4b, 5, and 7a, with typical acquisition times of 3 h and POM concentrations of 0.25 mM. Spectra measured for the L-Nle and D-Nle buffer blanks exhibit the expected Cotton effects in the UV range but nothing in the visible range, while racemic DL-Nle buffer is CD silent (Figure S16 in the Supporting Information).[89] Spectra measured for L-Nle containing 4b in L-Nle and D-NLe buffer, HCl (pH 2.4), and DMSO reveal Cotton effects associated with the electronic absorption transitions in the visible and UV ranges (Figure 5 and Figure S17 in the Supporting Information), indicating maintenance of chirality in solution in each case. The spectra in D-Nle and L-Nle buffer are of opposite sign, suggesting that exchange of the L-Nle ligands with bulk D-Nle from the buffer has occurred on the time scale of the experiment. In contrast, the retention of optical activity apparent from the spectra measured in DMSO and water suggest that the L-Nle ligands remain bound to the hybrid POM in these media and do not exchange rapidly with water or DMSO. Compound 5 possess racemic DL-Nle ligands,

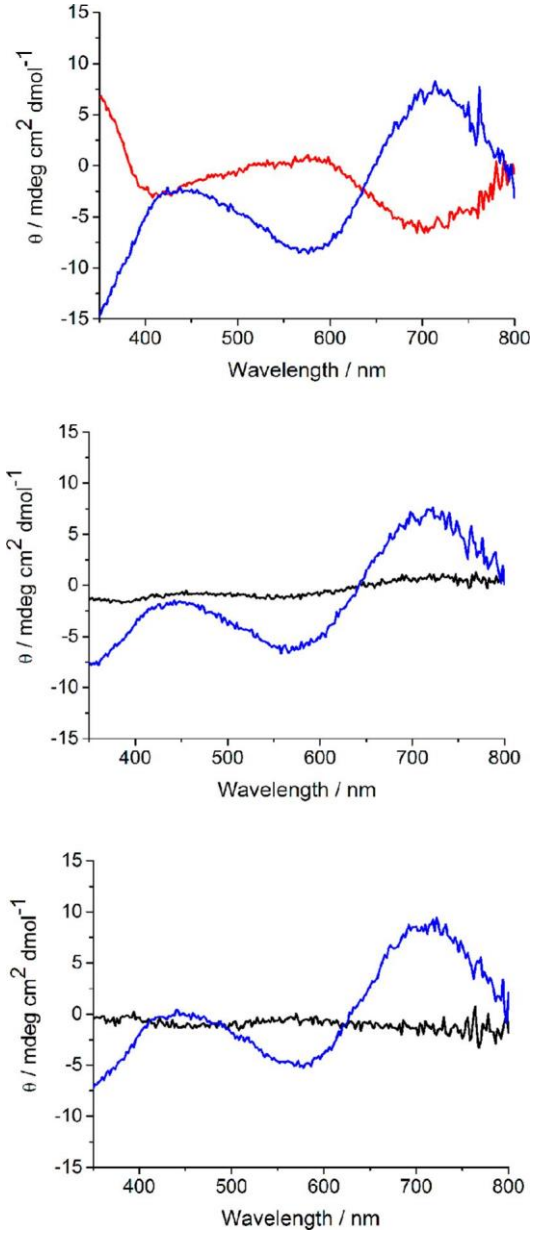

Figure 5. Circular dichroism spectra of (top) 0.25 mM solutions of 4b in 0.15 M L-Nle buffer (blue) and 0.15 M D-Nle buffer (red), (middle) 0.25 mM solutions of 5 in 0.15 M, pH 2.2 DL-Nle (black) and L-Nle (blue) buffer, and (bottom) 0.25 mM solutions of 7a in 0.2 M, pH 2.2 Gly buffer (black) and 0.15 M, pH 2.2 L-Nle buffer (blue).

and no Cotton effects are apparent in racemic DL-Nle buffer solution. However, upon dissolution of 5 in L-Nle buffer, the spectrum strongly resembles that of 4b in the same solution, again suggesting exchange of the racemic Nle ligands for enantiopure L-Nle ligands. Glycine-containing 7a is achiral in the solid state and in glycine buffer. However, the CD spectrum upon dissolution in L-Nle buffer also resembles that of 4b, indicating that the Gly ligands have been exchanged for L-Nle from the buffer. This amino acid exchange suggested by CD data has been confirmed by the synthesis of 7b following recrystallization of 4b from glycine buffer.

The measured CD spectra are all consistent with maintenance of coordinated amino acid ligands for the hybrid POMs in buffered and unbuffered aqueous media in the presence or absence of free amino acid and in DMSO. The data also suggest the exchange of amino acid ligands on the hybrid POMs with other amino acid ligands from buffer but minimal exchange for water or DMSO ligands. The Cotton effects are associated with the UV absorption bands of the oxo to metal LMCT bands and with the visible absorption bands assigned as $Mo^{V} \rightarrow Mo^{VI}$ and $Mo^{V} \rightarrow W^{VI}$ IVCT transitions of the reduced POM. Cotton effects associated with the $V^{IV} \rightarrow Mo^{V}$ IVCT bands of $[PMo_{11}V^{IV}O_{40}]^{5-}$ have been observed previously in the presence of chiral countercations.[49] It should be noted that the POM backbone of the present compounds is achiral in the absence of any amino acid ligands due to the approximate C_{2v} point symmetry. This is in contrast to literature examples where chiral tartrate or proline ligands enhance chirality in hybrid zirconium or lanthanoid phospho- and silicotungstates.[51−53] In the literature studies the POMs themselves are chiral and the effect is an overall enhancement of chirality by incorporation of chiral organic moieties, with each enantiomer of the organic species selectively binding to, or associating with, one enantiomeric form of the chiral POM.

NMR Spectroscopy. The synthesis of Gly-containing 7b from Nle-containing 4b and the CD results discussed above confirm the possibility of exchanging of amino acid ligands in this structural family of hybrid POMs, while retaining the POM framework. Previous studies of hybrid POMs incorporating carboxylate and other ligands have demonstrated the utility of ^{1}H NMR spectroscopy for studying ligand exchange in solution. In particular, 1D ^{1}H NMR spectra of the carboxylate-ligated Keplerate POMs exhibit distinct resonances for bound and unbound carboxylate ligands.[90−92]

Room-temperature ^{1}H NMR spectra of Nle-containing oxidized 3 and reduced 4b in D_2O are very similar (Figure S18 in the Supporting Information), and the spectra remain unchanged on the time scale of days. Distinct resonances are evident for each of the p-$MeBzNH_3^+$ and Nle/$NleH^+$ protons, with chemical shift values close to those of free Nle and p-$MeBzNH_2$. The integration values of these resonances are important for establishing the overall formulations of the compounds. The peaks in the ^{1}H NMR spectrum of 3 are sharp, the multiplicities due to coupling are evident, and there is no sign of paramagnetic broadening or shifting. The resonances measured for both the p-$MeBzNH_3^+$ and Nle/ $NleH^+$ moieties of 4b occur at the same chemical shifts as those for 3; however, the peaks attributed to the amino acid protons are somewhat broadened and a second set of very broad, lower intensity resonances are evident, shifted downfield. This second set of broader resonances integrates to approximately 30% of the main set and clearly indicates more than one environment for the Nle/$NleH^+$ moieties. Close inspection of the spectrum for 3 also reveals a similar additional set of resonances, although they are of much lower intensity for 3. Addition of free L-Nle to the solutions does not give rise to a set of distinct resonances for free Nle/$NleH^+$, instead increasing the intensity of the observed set of Nle/$NleH^+$ peaks. This is consistent with previous studies of the $[XMo_6O_{21}(AA)]^{n-}$ (X = Se^{IV}, Sb^{III}, Bi^{III}; AA = L-lysine or L-alanine) family, in which addition of free amino acid did not afford a separate set of for the amino acid protons.[50] This was attributed to either rapid ligand exchange or an insignificant chemical shift difference due to the minimum of four bonds separating the metal centers and amino acid protons. In order to probe the possibility of chemical exchange between free and bound Nle, variable-temperature spectra were measured for 3 in the temperature range 25−70 °C (Figure S19 in the Supporting Information). All of the peaks due to the p-

$MeBzNH_3^+$ cations and $Nle/NleH^+$ shift monotonically downfield with temperature, with no sign of decoalescence of exchanging protons. These observations indicate that exchange between free and bound $Nle/NleH^+$ must be fast on the ^1H NMR time scale at room temperature and above. No broadening is evident for the peaks corresponding to the p-$MeBzNH_3^+$ cations in the variable-temperature experiment. In contrast, the peaks associated with the Nle protons broaden upon heating and the extent of broadening appears to inversely correlate with the number of bonds from the Nle carboxylate group, with the peak due to the methine protons (δ 3.85 ppm at 25 °C) broadening most significantly. This may be ascribed to the effect of segmental motion along the carboxylate-tethered aliphatic n-butyl side chain of the Nle ligands and the temperature-induced increased rate of tumbling of the macromolecular hybrid POM.[93] Variable-temperature ^1H NMR spectra measured for 4b were similar to those measured for 3; notably, the additional lower intensity broad set of resonances associated with the $Nle/NleH^+$ protons shifts as per the higher intensity, sharper set, but they do not broaden and the two sets did not coalesce (Figure S20 in the Supporting Information).

The $^{13}C\{^1H\}$ NMR spectra of 3 and 4b in D_2O (Figures S21 and S22 in the Supporting Information), acquired overnight on a high resolution 800 MHz spectrometer on nearly saturated samples, shows the resonances for the p-$MeBzNH_3^+$ cations and $Nle/NleH^+$ moieties at the typical chemical shift values. As per the ^1H NMR spectrum, there is an additional lower intensity set of resonances associated with the $Nle/NleH^+$ resonances, which are downfield from the main peaks and more intense for 4b than for 3. To ascertain whether additional sets of ^1H and ^{13}C resonances are correlated, a 2D ^1H–^{13}C heteronuclear single quantum coherence (HSQC) spectrum was also collected for 4b in D_2O (Figures S23 and S24 in the Supporting Information). In addition to the expected single cross peak for each of the p-$MeBzNH_3^+$ cation C atoms, the HSQC spectrum exhibits cross peaks between the major and minor sets of resonances associated with the $Nle/NleH^+$ moieties, and the major sets of ^1H and ^{13}C resonances correlate with each other, as do the minor sets of ^1H and ^{13}C. Overall, this spectrum suggests up to four different $Nle/NleH^+$ environments (Figure S24). These are most obvious for the α-C(H) and β-C(H_2) groups, which exhibit three and four clear sets of cross peaks, respectively. In addition to three distinct types of bound Nle ligands (two bidentate and one monodentate; Figure S3 in the Supporting Information), free $NleH^+$ countercations as well as free Nle zwitterions may exist in solution, which can account for the multiple observed species. The relatively higher intensities of the additional resonances for 4b versus 3 is consistent with the absence from 3 of the monodentate Nle ligand and free zwitterionic norleucine that are present in 4b.

Electrochemistry. Having established with SAXS and CD spectroscopy the solution stability of the reduced hybrid Gly and Nle POMs in certain media, voltammetric and coulometric studies were undertaken to determine the degree of reduction and explore the possibility of interconverting between the oxidized and reduced analogues. Electrochemical studies of the $\{Mo^V_2\}$-containing reduced Nle-containing species 4a–c and 5 were performed in DMSO (0.05 M Bu_4NPF_6), due to the strong adsorption of the complexes on the electrode surface in aqueous media (Figure 6 and Figure S25 and S26 in the Supporting Information). Small-angle X-ray scattering suggests

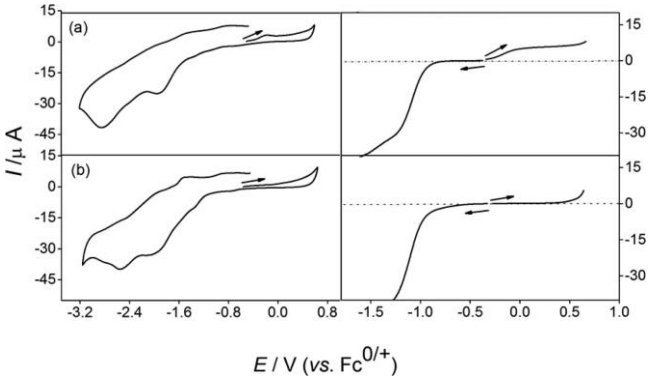

Figure 6. Cyclic (left) and RDE (right) voltammograms of Nle-containing compounds (a) 4b and (b) 4b following oxidative electrolysis. For CV ν = 100 mV s^{-1}, and for RDE ν = 20 mV s^{-1} and ω = 104.7 s^{-1}.

that oxidized analogue 3 is unstable in DMSO, which prevents comparison of electrochemical data. Transient cyclic voltammograms for all the chemically reduced analogues 4a–c and 5 show an irreversible oxidative process at all the scan rates (0.05–1 V s^{-1}) studied, with a peak potential, E_p, of around −0.19 V at a scan rate, ν, of 100 mV s^{-1}. All compounds exhibit at least two irreversible reductive processes at potentials more negative than −0.5 V, which could be assigned to the reduction of the W or Mo centers. Details of these reduction processes are not discussed here, as they are beyond the focus of this study. The near steady-state mass transport limiting currents associated with the oxidative process for compounds 4a–c are similar after the concentrations are taken into account, suggesting similar degrees of reduction. In addition, the limiting current of the oxidative process is less than half of that of the first reductive process. After exhaustive oxidative electrolysis of 4b,c at −0.01 V, the solution changed from dark blue to colorless, and no oxidation process was observed in both cyclic and RDE voltammograms, confirming complete oxidation of all Mo^V to Mo^{VI}. The charge consumed during the oxidative electrolysis is consistent with oxidation by 1.8(2) electrons per polyanion for both compounds. The voltammograms obtained after electrolysis do not exhibit a reductive process at a potential similar to the oxidative process in the parent compound, indicating that it is not possible to electrochemi-cally interconvert between $\{Mo^V_2\}$-containing 4b,c and a homovalent analogue with a $\{Mo^{VI}_3W^{VI}\}$ core, which is consistent with the irreversible nature of the process observed from voltammetry. Exhaustive oxidative electrolysis of 5 at −0.01 V again converts the solution from dark blue to colorless, with the disappearance of the oxidation process in both cyclic and RDE voltammograms measured after the electrolysis, confirming complete oxidation of all Mo^V to Mo^{VI}. The charge passed is consistent with oxidation by 1.3(2) electrons per polyanion. The different numbers of electrons measured by coulometry of 4b,c versus 5 is consistent with the extinction coefficients from the electronic absorption spectra (see above) and the composition of 5 involving a proportion of 2e-reduced polyanions smaller than that for 4b,c.

Transient cyclic and steady-state rotating disk electrode (RDE) voltammograms (Figure 7) were also measured on freshly prepared solutions of Gly-containing 6 and 7a,b (0.3 mM polyanion, in 0.2 M Gly buffer, pH 2.2). These compounds were measured in aqueous solution because they are insoluble in DMSO and no electrode adsorption problems

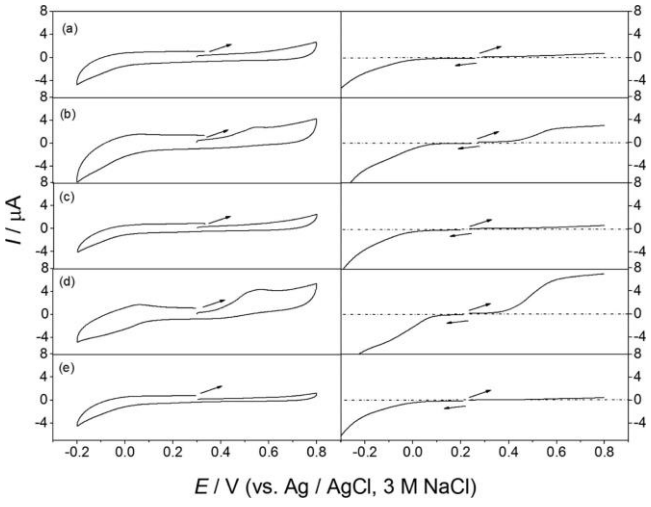

Figure 7. Cyclic (left) and RDE (right) voltammograms of 0.3 mM Gly-containing compounds (a) 6, (b) 7a, (c) 7a following oxidative electrolysis, (d) 7b, and (e) 7b following oxidative electrolysis in 0.2 M Gly buffer, pH 2.2. For CV ν = 100 mV s^{-1}, and for RDE ν = 20 mV s^{-1} and ω = 104.7 s^{-1}.

are apparent. Again $\{Mo^{V}_2\}$-containing reduced analogues 7a,b exhibit an irreversible oxidative process at all scan rates (0.05−1 V s^{-1}) studied, with an E_p value of +0.54 V at ν of 100 mV s^{-1}, while no equivalent reductive process was observed for the oxidized analogue 6. The magnitude of the steady-state mass transport limiting current associated with the oxidative process for 7a is approximately half of that for 7b, indicating that 7b is comprised of a significantly larger proportion of 2e-reduced $\{Mo^{V}_2\}$-containing POM. As for the Nle-containing species, exhaustive electrolysis of 7a,b at +0.6 V again converts the solutions from dark blue to colorless, with the close to zero current measured in the positive potential range in the RDE voltammogram after the electrolysis confirming complete oxidation. The charge passed indicates oxidation by 0.7(2) and 1.5(2) electrons per polyanion for 7a,b, respectively, as the fraction of 2e-reduced POM in each compound is oxidized. The lesser degree of reduction apparent for 7a versus 7b from the RDE limiting currents and coulometry is consistent with the electronic absorption spectra. Neither 6 nor electrochemically oxidized 7a,b exhibits a reduction process in the potential range similar to the oxidation process of 7a, suggesting that electrochemical interconversion of these hybrid POMs is not possible, as per the norleucine analogues.

Density Functional Theory (DFT) Calculations. Density functional theory calculations were employed to probe the trends observed experimentally concerning the relative stabilities of the different hybrid POM analogues and positional isomers and the facility of their reduction. To save computa-tional time, simplified model compounds with no terminal aqua ligands and formate ligands instead of amino acid ligands were employed for all calculations. Complexes with a trimetallic core were thus modeled as $[As_4(M^{VI}_3)M^{VI}_{44}Y_4O_{159}(O_2CH)_8]^{20-}$ (M = Mo, W, abbreviated as $\{Mo_3\}Mo_xW_{44-x}$ and $\{W_3\}Mo_xW_{44-x}$), while those with a tetrametallic core were modeled as $[As_4(M^{VI}_4)M^{VI}_{44}Y_4O_{160}(O_2CH)_8]^{16-}$ (abbreviated as $\{Mo_yW_{4-y}\}W_{44}$ and $\{Mo_yW_{4-y}\}Mo_xW_{44-x}$).

$\{Mo_3\}Mo_xW_{44-x}$ Compounds. Crystallographic data (see above) for all characterized compounds indicate a very marked preference for the location of Mo atoms in the central tri- or tetrametallic core, over all other structural sites (Table S6 and Figure S2 in the Supporting Information). Calculations are consistent with this observation, with total binding energy values for the pair of positional isomers $\{Mo_3\}W_{44}$ and the hypothetical $\{W_3\}Mo_3W_{41}$ confirming that the former is the most stable by 14.7 kcal mol^{-1} (Table S6). Thus, on average, each Mo center in a core site is ca. 5 kcal mol^{-1} more stable than that in a "non-core" site. The origin for this trend is unclear, although it is likely related to subtle differences in the radii of $Mo^{V/VI}$ and $W^{V/VI}$ versus the size of the internal metal−oxo core defined by the external POM framework.

The preference for localization of the Mo atoms in the central core above all other sites is very clear. However, all of the crystallographically characterized compounds described

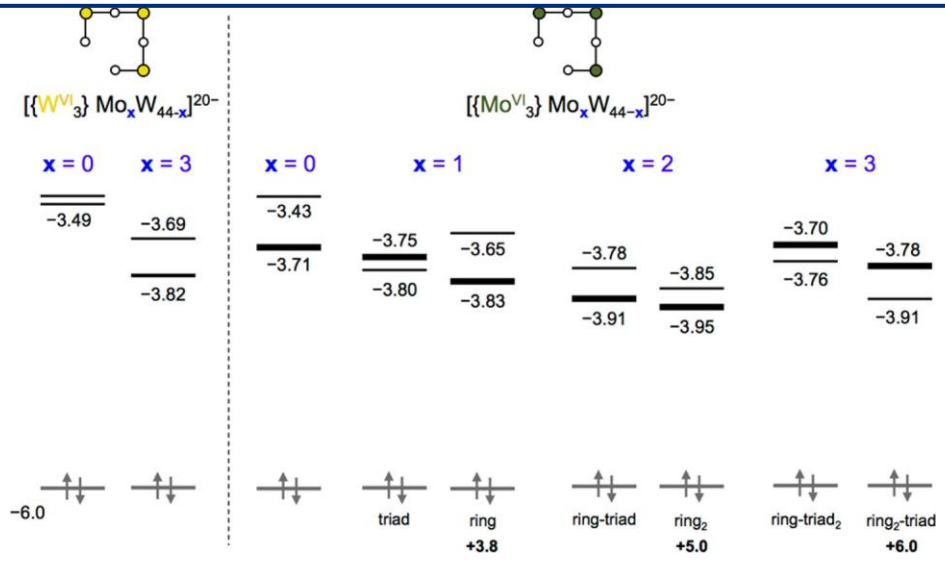

Figure 8. Electronic structure of fully oxidized $[\{W_3\}Mo_xW_{44-x}]^{20-}$ (x = 0 and 3) and $[\{Mo_3\}Mo_xW_{44-x}]^{20-}$ (x = 0−3) systems in aqueous solution. The HOMO (gray), LUMO, and LUMO+1 energies (in eV) are shown, with thick lines representing orbitals localized on the $\{Mo_3\}$ core (see Figure S14 in the Supporting Information). Below the HOMOs, the localization (triad or ring) of the x external Mo atoms is indicated, together with the binding energy differences (kcal mol^{-1}) between compounds with the same x value.

above also possess between 0.5 and 2.5 additional Mo atoms disordered with W atoms in the external non-core POM framework, with a further preference for localization of Mo in the $\{Y_4M_8L_8\}$ "ring" and $\{AsM_9\}$ "triad" sites over the $\{AsM_9\}$ "belt" (Figure S2 in the Supporting Information). Several different positional isomers of the $\{Mo_3\}Mo_xW_{44-x}$ ($x = 0-3$) series were calculated to explore this aspect, with the Mo atoms occupying different sites. The calculated binding energies and interatomic parameters are reported in Tables S12 and S3 in the Supporting Information, respectively. In general, all of the optimized $\{Mo_3\}Mo_xW_{44-x}$ structures exhibit longer intera-tomic distances and wider bond angles than are apparent from the single-crystal structural data for homologous 3w (Table S7 in the Supporting Information), with the exception of the terminal M O distance. This fact suggests that the optimized geometry is naturally expanded with respect to the crystal structure. This is a well-known tendency in solution, which is the approach taken to compute the optimized structures via a continuum solvent model. Another source of discrepancy between the crystallographic and computed structures is that the experimental interatomic distances of the internal square core are averaged over the four sites, including the vacancy. It is worth mentioning that the computed M−O(−M) distances show a wide range of values, reminiscent of the Mo−O−Mo alternating bond length feature characteristic of polyoxomolyb-dates,[94] which are not apparent in the crystallographic data due to the effect of averaging over the equivalent sites.

The frontier orbital energies of the $\{Mo_3\}Mo_xW_{44-x}$ series and the difference in total binding energy between the positional isomers with the same x value are presented in Figure 8, along with frontier orbital energies for two members of the hypothetical $\{W_3\}Mo_xW_{44-x}$ series, for comparison. For $x = 1$, the form with the external Mo located in a $\{AsM_9\}$ triad is 3.8 kcal mol^{-1} more stable than that with Mo in the $\{Y_4M_8L_8\}$ ring. For $x = 2$, $\{Mo_3\}Mo(ring)Mo(triad)W_{42}$ is 5 kcal mol^{-1} more stable than $Mo(ring)_2W_{42}$. For the hypothetical 2e-reduced forms of $\{Mo_3\}Mo_xW_{44-x}$ with $x = 1, 2$ we compute $E = 2.1$ and 0.073 kcal mol^{-1}, respectively. This latter trend is consistent with the lowest unoccupied molecular orbitals (LUMOs) of the least stable oxidized forms. For $x = 3$, $\{Mo_3\}Mo_2(ring)Mo(triad)W_{41}$ is estimated to be 6.0 kcal mol^{-1} less stable than $\{Mo_3\}Mo(ring)Mo_2(triad)W_{41}$. Thus, for all $\{Mo_3\}Mo_xW_{44-x}$ compounds with $x > 0$, the external Mo centers exhibit a thermodynamic preference for the triad positions of $\{AsM_9\}$ over the $\{Y_4M_8L_8\}$ ring positions in all cases calculated. However, this contrasts with the crystallographic analysis, namely the higher Mo occupancy of ring positions in comparison with triad positions, a fact likely ascribed to kinetic rather than thermodynamic control during synthesis and crystallization.

In Figure 8, the fully oxidized $\{Mo_3\}Mo_xW_{44-x}$ and $\{W_3\}Mo_xW_{44-x}$ compounds (charge $q = -20$) feature highest occupied molecular orbitals (HOMOs) at a constant energy of −6.0 eV, irrespective of the composition of the external Mo_xW_{44-x} framework. That is, the number of Mo centers in the external framework does not affect the energies of the HOMOs. The LUMOs feature a slow tendency to stabilize as the composition of the external "non-core" framework of $\{Mo_3\}$ Mo_xW_{44-x} becomes richer in Mo (x varying from 0 to 3), which is also apparent for the two hypothetical $\{W_3\}Mo_xW_{44-x}$ species ($x = 0, 3$). This trend follows the evidence reported for other mixed-metal POMs, for which LUMO energies typically decrease (concomitantly increasing the oxidizing power) as the Mo/W ratio increases.[95] Taking $\{Mo_3\}W_{44}$ as a reference, the LUMO at −3.7 eV is fully localized on the internal Mo-based trinuclear core (Figure S27 in the Supporting Information). Increasing the number of non-core Mo centers in $\{Mo_3\}Mo_xW_{44-x}$ changes the nature of the lowest energy metal-based orbitals. As the LUMO associated with $\{Mo_3\}$ is rather high in energy, the presence of noncore Mo atoms can vary the localization of the LUMO. Calculations suggest this is the case for $\{Mo_3\}Mo(triad)W_{43}$ and $\{Mo_3\}$ $Mo(ring)Mo(triad)_2W_{41}$ (Figure S27), for which the LUMOs are located on Mo centers in the peripheral $\{AsM_9\}$ units of the POM framework. This is not the case for the $\{Mo_3\}Mo(ring)$ W_{43} or $\{Mo_3\}Mo_2W_{42}$ systems, for which the LUMO remains localized on the trinuclear core.

Comparison of $\{Mo_3\}$ and $\{Mo_yW_{4-y}\}$ Cores. In this work, we have modeled the hybrid POM structures containing a trimetallic $\{Mo_3\}$ core, which are compared with analogous calculations recently communicated by some of us for analogues with tetrametallic $\{Mo_yW_{4-y}\}$ cores.[54] Recalling these theoretical results, we observe that the number of core Mo atoms (y) strongly affects the electronic affinity and reducibility of the POM. From $\{W_4\}$ to $\{Mo_4\}$, the absolute energies of the LUMOs gradually decrease in energy by 0.7 eV in total (Figure 9). Thus, we concluded that the $\{Mo_4\}$ and

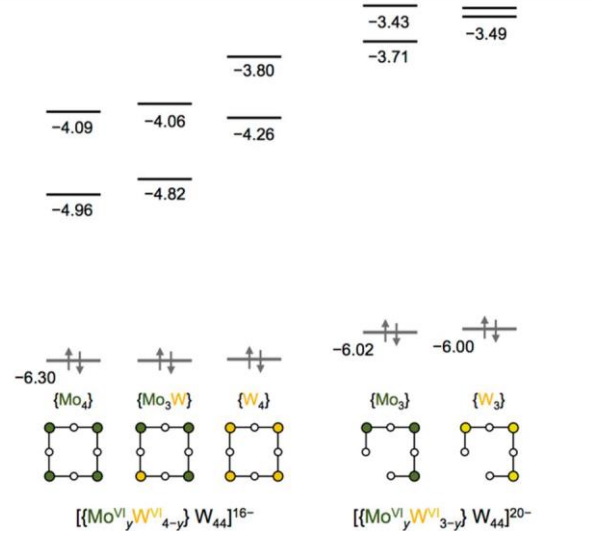

Figure 9. Frontier molecular orbital energies (eV) computed for the structures indicated. The central $\{M_4\}$ or $\{M_3\}$ core is shown schematically (color code: W, yellow; Mo, green; O, white).

$\{Mo_3W\}$ species are readily reduced and accommodate two paired electrons in the core. The reduced $\{Mo^V_2W^{VI}_2\}$ species is likely also accessible. On the other hand, the calculations indicate that species with $\{Mo_yW_{4-y}\}$ ($y < 2$) cores are considerably more difficult to reduce and we have no experimental evidence for the formation of these analogues. It must be noted that, for all $\{Mo_yW_{4-y}\}Mo_xW_{44-x}$ species, the Mo/W composition of the noncore POM framework does not affect the redox state of the POM or its ease of reduction. This is due to the comparatively high energy of the first empty orbital that is localized on the noncore part of the POM framework. These theoretical results are in good agreement with the present experimental findings regarding the facility of reduction of the analogues with a tetrametallic core.

Let us now compare the formally fully oxidized (hexavalent Mo^{VI}/W^{VI}) $\{Mo_3\}W_{44}$ and $\{W_3\}W_{44}$ species with $\{Mo_4\}W_{44}$ structures in aqueous solution (the optimized DFT geometries of $\{Mo_3\}W_{44}$ and $\{Mo_4\}W_{44}$ can be found in Table S8 in the Supporting Information). The LUMO and HOMO are found at −3.71 and −6.02 eV for $\{Mo_3\}W_{44}$, whereas the values are −3.49 and −6.00 eV for $\{W_3\}W_{44}$ (Figure 9). For $\{Mo_3\}W_{44}$ the LUMO and LUMO+1 are localized on the internal trinuclear core (Figure 10), at variance with hypothetical

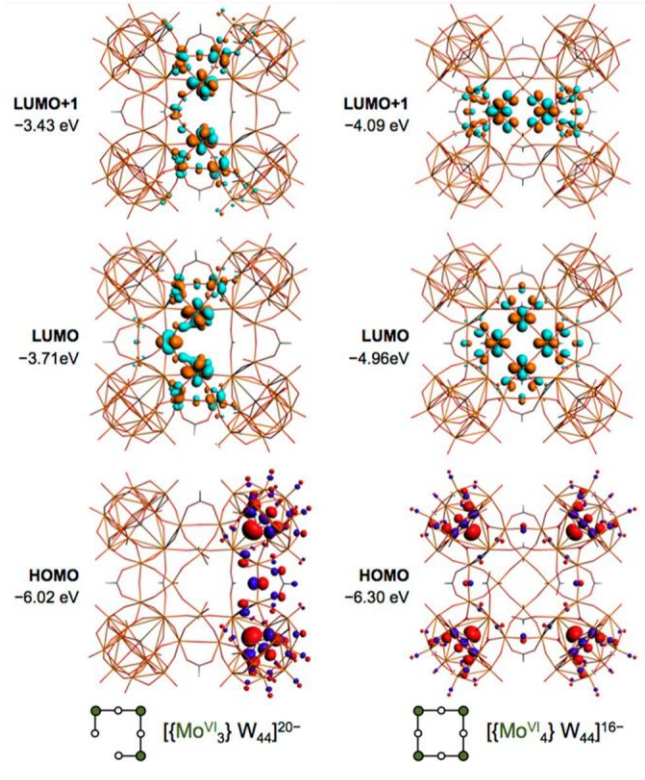

Figure 10. Frontier orbitals (3D representation and energy) computed for fully oxidized $\{Mo_3\}W_{44}$ (q = −20) and $\{Mo_4\}W_{44}$ (q = −16). Although the orbitals are similarly localized and have the same nature in both compounds, the different molecular charges and the open/closed arrangement of the central loop afford the large energy differences (in eV) notably for LUMOs and LUMO+1s.

compounds based on the $\{W_3\}$ internal moiety (see LUMO and LUMO+1 in Figure S28 in the Supporting Information, left). In the $\{Mo_yW_{4-y}\}W_{44}$ systems, with the tetranuclear core (q = −16), the homologous orbitals are found at −4.26/−6.30 eV for $\{W_4\}W_{44}$, at −4.82/−6.30 eV for $\{Mo_3W\}W_{44}$, and at −4.96/−6.30 eV for $\{Mo_4\}W_{44}$. In all cases, the HOMO is located on the $\{AsO_3\}$ heteroatomic groups of the peripheral lacunary Keggin moieties and the LUMO is localized on the internal metal−oxo square core. From $\{Mo_yW_{4-y}\}W_{44}$ to $\{Mo_3\}W_{44}$, the energy change in the HOMO is minor (0.27 eV), whereas the LUMO of $\{Mo_3\}W_{44}$ is 1.25 eV higher than that of $\{W_4\}W_{44}$, which is the highest of all species with a tetranuclear core. The change in the HOMO energy arises mainly from the molecular charge variation, and it is modest due to the relatively high nuclearity of the system, which largely dissipates the charge effect. On the other hand, removal of one metal center from the central square core has dramatic consequences on the LUMOs, which are localized on the core as well. Accepting that the pure charge effect applies similarly to the occupied and unoccupied orbitals, the larger energy change for the unoccupied orbitals must originate from the effect of the "broken" or incomplete internal loop, because of the missing $\{MO\}^{4+}$ unit. Thus, the extra stability of the associated LUMOs conferred by the closed $\{Mo_yW_{4-y}\}$ metal− oxo loop is absent for the $\{Mo_3\}Mo_xW_{44-x}$ series with the trinuclear core. A similar stabilizing effect of closed metal−oxo rings has been previously reported by some of us for other POMs.[96] The main effect of loop opening is a large increase in energy for the MOs localized on the internal core, which includes the orbitals that will accept electrons upon reduction. These theoretical results explain why the $\{Mo_3\}Mo_xW_{44-x}$ family is intrinsically more difficult to reduce (i.e. accommodate metal-based electrons) than any $\{Mo_yW_{4-y}\}Mo_xW_{44-x}$ ana-logue. This is consistent with the experimental observation that the compounds with the trinuclear $\{Mo_3\}$ core are invariably obtained in the oxidized hexavalent (Mo^{VI}/W^{VI}) form under ambient conditions, while the analogues with the tetranuclear form are prone to reduction. For comparison purposes, the $[PW_{12}O_{40}]^{3-}$ Keggin and $[P_2W_{18}O_{62}]^{6-}$ Wells−Dawson anions, two well-known POMs that are readily reduced, have LUMOs of around −4.4 eV in aqueous solution:[97] that is, as much as 0.7 eV lower than $\{Mo_3\}W_{44}$. From the point of view of molecular stability, we suggest that nonreducible POMs, such as the $\{Mo_3\}$-containing species 3 and 6, are less stable than the readily reduced $\{Mo_yW_{4-y}\}$-containing species, such as 4, 5, and 7.

The compounds 4, 5, and 7 are formulated as partially (5 and 7) or fully (4) comprised of a tetranuclear 2e-reduced species, formulated as $\{Mo^V_2Mo^{VI}W\}$. As discussed above, the available experimental data do not allow us to distinguish between a single POM with a $\{Mo^V_2Mo^{VI}W\}$ core and an equal mixture of POMs with $\{Mo^V_2Mo^{VI}_2\}$ and $\{Mo^V_2W^{VI}_2\}$ cores. We have computed the 2e-reduction reaction energies for the fully oxidized, hexavalent species corresponding to both cases and found an energy difference of only 1 kcal mol^{-1} in favor of a 50:50 mixture of species with $\{Mo^V_2Mo^{VI}_2\}$ and $\{Mo^V_2W^{VI}_2\}$ cores. However, the modest size of this energy difference is insufficient to provide full clarification of this point.

CONCLUDING REMARKS

A comprehensive investigation of a family of heterometallic POMs with amino acid ligands indicates a robust POM framework that is readily modified in terms of the nuclearity of the metal−oxo core, the metal composition, the redox state and the amino acid ligands. In the absence of visible light or a chemical reductant, the reaction product is the fully oxidized homovalent Mo^{VI}/W^{VI}-containing hybrid POM with a trinuclear $\{Mo^{VI}_3\}$ core, while light-induced or chemical reduction affords species with a tetrametallic core, with varying proportions of an overall 2e-reduced species with a $\{Mo^V_2M^{VI}_2\}$ core (M = Mo, W) mixed with the oxidized hexavalent analogue. The reduced compounds exhibit the dark blue color characteristic of classical "heteropoly blues" and are diamagnetic with the two additional electrons strongly antiferromagnetically coupled. These reduced compounds are air stable in the solid state. They can be oxidized in solution, affording analogues that are unstable and cannot be reduced back to the original complex. This behavior is reminiscent of the Mo-blue giant wheels, the fully oxidized Mo^{VI} analogues of which are not accessible. In contrast to the analogues with a tetrametallic core, those with a trimetallic $\{M_3\}$ core are not readily reduced. This is consistent with DFT calculations that

indicate that the LUMO is much higher in energy for hexavalent analogues with the $\{M_3\}$ versus $\{M_4\}$ core. For complexes with the tetrametallic core, the $\{M_4\}$ closed loop confers extra stability on the LUMO associated with this moiety, resulting in facile 2e reduction and accommodation of the two electrons in this MO. This reduction is so facile that a fully oxidized analogue with a hexavalent tetrametallic core cannot be isolated. In contrast, the $\{M_3\}$ open loop affords much higher energies for the LUMO and LUMO+1, with no reduction process evident for complexes with the trimetallic core. This observation is analogous to linear and ring-conjugated π systems, where the orbital energies of the π system are lower in rings: i.e., aromatic molecules. Preferential Mo substitution for the different Mo/W POM sites is also clearly evident, with the central core significantly more favored for Mo than any of the other POM positions. This is the site of 2e reduction and is consistent with the more facile reduction of the 5d transition metal Mo versus its 6d congener W.

While SAXS studies are consistent with maintenance of the metal−oxo POM framework in solution under defined conditions, determining whether the amino acid ligands remain coordinated in solution was also of interest at the outset of this study. Circular dichroism experiments indicate that the α-amino acid ligands remain associatedwith the POM framework in solution but undergo exchange with free α-amino acid molecules. This exchange is fast on the ^{1}H NMR time scale. Amino acid ligand exchange has been definitively demonstrated by the synthesis of a glycine-containing hybrid POM directly from a norleucine-containing analogue. In contrast, the amino acid ligands do not appear to undergo rapid exchange with water or DMSO. In general, concentrated solutions of the hybrid POMs retain their structure in aqueous solution within a defined pH range (POM to proton concentration ratio) on the time scale of days. The stability is greater in the presence of excess α-amino acid, and generally the reduced species are more stable than the oxidized. After 1 week in solution (no excess of amino acid), electronic absorption, CD, and SAXS studies indicate decomposition of the POM; SAXS suggests that this is decomposition to a smaller POM and not to simple mono-oxanions. In contrast, in the presence of excess amino acid, SAXS shows some evidence of aggregation after 1 week in some cases, corresponding to the formation of the well-known POM "blackberries" or "vesicles", which is a subject of ongoing investigation.

Finally, despite the accessibility of stable 2e-reduced analogues, this structural family of hybrid POMs is not promising for redox catalysis because the system is not amenable to reversible interconversions between the oxidized and reduced forms. However, in principle, similar POMs with accessible photoreduced forms that can be readily cycled between oxidized and reduced states may prove important for efficient photoreduction catalysis because they do not require an additional photosensitizer as cocatalyst. This work highlights the potential of mixed-metal hybrid POMs in this regard and reveals the importance of several key structural features in stabilizing the reduced analogues. Clearly useful are neutral zwitterionic amino acids rather than anionic carboxylate ligands, which serve to minimize the overall negative charge of the hybrid POM and thereby facilitate reduction. Also potentially valuable are "closed metal−oxo loops" of Mo centers that are preferentially reduced and can act as electron reservoirs in mixed-metal molybdotungstates. The challenge remains to synthesize hybrid POMs that strike the right balance between these structural features to afford stability to both oxidized and reduced partners but also allow facile interconversion between them.

ASSOCIATED CONTENT

* Supporting Information

The Supporting Information is available free of charge on the ACS Publications website at DOI: 10.1021/acs.inorgchem.6b02218.

Additional structural, spectroscopic, electrochemical, and computational data (PDF)

X-ray crystallographic data for 3w, 4aw−4cw, and 7aw,bw (CIF)

AUTHOR INFORMATION

Corresponding Author

*E-mail for C.B.: c.boskovic@unimelb.edu.au.

Notes

The authors declare no competing financial interest.

ACKNOWLEDGMENTS

We thank Andy Ohlin for helpful discussions; David Tiede and Xiaobing Zuo for providing the SolX program, Hamish Grant and Matthew Field for assistance with the NMR and XPS, respectively, the Australian Research Council for funding (DP110100155), the Spanish MINECO (project CTQ2014-52774-P), the DGR of the Generalitat de Catalunya (grant no. 2014SGR199), and the XRQTC.

REFERENCES

(1) Nagul, E. A.; McKelvie, I. D.; Worsfold, P.; Kolev, S. D. The molybdenum blue reaction for the determination of orthophosphate revisited: Opening the black box. Anal. Chim. Acta 2015, 890, 60−82.

(2) Kozhevnikov, I. V. Catalysis by Polyoxometalates; Wiley: Chichester, England, 2002.

(3) Pope, M. T. Heteropoly and Isopoly Oxometalates; Springer-Verlag: Berlin, Germany, 1983.

(4) Rinfray, C.; Renaudineau, S.; Izzet, G. Proust, A covalent polyoxomolybdate-based hybrid with remarkable electron reservoir properties. Chem. Commun. 2014, 50, 8575−8577.

(5) Lv, H.; Geletii, Y. V.; Zhao, C.; Vickers, J. W.; Zhu, G.; Luo, Z.; Song, J.; Lian, T.; Musaev, D. G.; Hill, C. L. Polyoxometalate water oxidation catalysts and the production of green fuel. Chem. Soc. Rev. 2012, 41, 7572−7589.

(6) Yamase, T. Photo- and Electrochromism of Polyoxometalates and Related Materials. Chem. Rev. 1998, 98, 307−326.

(7) Streb, C. New trends in polyoxometalate photoredox chemistry: from photosensitisation to water oxidation catalysis. Dalton Trans. 2012, 41, 1651−1659.

(8) Bernardini, G.; Wedd, A. G.; Zhao, C.; Bond, A. M. Photochemical oxidation of water and reduction of polyoxometalate anions at interfaces of water with ionic liquids or diethylether. Proc. Natl. Acad. Sci. U. S. A. 2012, 109, 11552−11557.

(9) Kogan, V.; Aizenshtat, Z.; Neumann, R. Polyoxometalates as reduction catalysts: Deoxygenation and hydrogenation of carbonyl compounds. Angew. Chem., Int. Ed. 1999, 38, 3331−3334.

(10) von Allmen, K.; Moré, R.; Müller, R.; Soriano-Lopez, J.; Linden, A.; Patzke, G. R. Nickel-Containing Keggin-Type Polyoxometalates as Hydrogen Evolution Catalysts: Photochemical Structure-Activity Relationships. ChemPlusChem 2015, 80, 1389−1398.

(11) Troupis, A.; Hiskia, A.; Papaconstantinou, E. Angew. Chem., Int. Ed. 2002, 41, 1911−1914.

(12) Wang, Y.; Neyman, A.; Arkhangelsky, E.; Gitis, V.; Meshi, L.; Weinstock, I. Self-assembly and structure of directly imaged inorganic-

anion monolayers on a gold nanoparticle. J. Am. Chem. Soc. 2009, 131, 17412−17422.
(13) Mitchell, S. G.; de la Fuente, J. M. The synergistic behavior of polyoxometalates and metal nanoparticles: from synthetic approaches to functional nanohybrid materials. J. Mater. Chem. 2012, 22, 18091− 18100.
(14) Poblet, J. M.; Lopez, X.; Bo, C. Ab initio and DFT modelling of complex materials: towards the understanding of electronic and magnetic properties of polyoxometalates. Chem. Soc. Rev. 2003, 32, 297−308.
(15) Lopez, X.; Carbo, J. J.; Bo, C.; Poblet, J. M. Structure, properties and reactivity of polyoxometalates: a theoretical perspective. Chem. Soc. Rev. 2012, 41, 7537−7571.
(16) Sadakane, M.; Steckhan, E. Electrochemical Properties of Polyoxometalates as Electrocatalysts. Chem. Rev. 1998, 98, 219−238.
(17) Eda, K.; Osakai, T. How Can Multielectron Transfer Be Realized? A Case Study with Keggin-Type Polyoxometalates in Acetonitrile. Inorg. Chem. 2015, 54, 2793−2801.
(18) Aparicio, P. A.; Poblet, J. M.; Lopez, X. Tungsten redox waves in $[XMW_{11}O_{40}]^{n-}$ (X = P, Si, Al and M = W, Mo, V, Nb, Ti) Keggin compounds - Effect of localised/delocalised charges. Eur. J. Inorg. Chem. 2013, 2013, 1910−1916.
(19) Müller, A.; Krickemeyer, E.; Meyer, J.; Bögge, H.; Peters, F.; Plass, W.; Diemann, E.; Dillinger, S.; Nonnenbruch, F.; Randerath, M.; Menke, C. $[Mo_{154}(NO)_{14}O_{420}(OH)_{28}(H_2O)_{70}]^{(25\pm5)-}$: A Water-Soluble Big Wheel with More than 700 Atoms and a Relative Molecular Mass of About 24000. Angew. Chem., Int. Ed. Engl. 1995, 34, 2122−2124.
(20) Müller, A.; Serain, C. Soluble Molybdenum Blues. Acc. Chem. Res. 2000, 33, 2−10.
(21) Müller, A.; Das, S. K.; Krickemeyer, E.; Kuhlmann, C. Polyoxomolybdate Clusters: Giant Wheels and Balls. Inorg. Synth. 2004, 34, 191−200.
(22) Baker, L. C. W.; Glick, D. C. Present General Status of Understanding of Heteropoly Electrolytes and a Tracing of Some Major Highlights in the History of Their Elucidation. Chem. Rev. 1998, 98, 3−50.
(23) Varga, G. M., Jr Heteropoly blues. IV. Spectroscopic and magnetic properties of some reduced polytungstates. Inorg. Chem. 1970, 2003, 662−667.
(24) Prados, R. A.; Pope, M. T. Low-temperature electron spin resonance spectra of heteropoly blues derived from some 1:12 and 2:18 molybdates and tungstates. Inorg. Chem. 1976, 15, 2547−2553.
(25) Kozik, M.; Hammer, C. F.; Baker, L. C. W. Direct Determination by ^{183}W NMR of the Locations of Added Electrons in ESR-Silent Heteropoly Blues. Chemical Shifts and Relaxation Times in Polysite Mixed-Valence Transition-Metal Species. J. Am. Chem. Soc. 1986, 108, 2748−2749.
(26) Kozik, M.; Casan-Pastor, N.; Hammer, C. F.; Baker, L. C. W. Ring Currents in Wholly Inorganic Heteropoly Blue Complexes. Evaluation by a Modification of Evans's Susceptibility Method. J. Am. Chem. Soc. 1988, 110, 7697−770.
(27) Proust, A.; Matt, B.; Villanneau, R.; Guillemot, G.; Gouzerh, P. Izzet, Functionalization and post-functionalization: a step towards polyoxometalate-based materials. Chem. Soc. Rev. 2012, 41, 7605− 7622.
(28) Dolbecq, A.; Dumas, E.; Mayer, C. R.; Mialane, P. Hybrid organic-inorganic polyoxometalate compounds: from structural diversity to applications. Chem. Rev. 2010, 110, 6009−6048.
(29) Santoni, M.-P.; Hanan, G. S.; Hasenknopf, B. Covalent multi-component systems of polyoxometalates and metal complexes: Toward multi-functional organic−inorganic hybrids in molecular and material sciences. Coord. Chem. Rev. 2014, 281, 64−85.
(30) Bassil, B. S.; Kortz, U. Z. Recent Advances in Lanthanide-Containing Polyoxotungstates. Z. Anorg. Allg. Chem. 2010, 636, 2222− 223.
(31) Vonci, M.; Boskovic, C. Polyoxometalate-Supported Lanthanoid Single-Molecule Magnets. Aust. J. Chem. 2014, 67, 1542−1552.
(32) Reinoso, S. Heterometallic 3d-4f polyoxometalates: still an incipient field. Dalton Trans. 2011, 40, 6610−6615.
(33) Ma, X.; Yang, W.; Chen, L.; Zhao, J. Significant developments in rare-earth-containing polyoxometalate chemistry: synthetic strategies, structural diversities and correlative properties. CrystEngComm 2015, 17, 8175−8197.
(34) Miras, H. N.; Stone, D. J.; McInnes, E. J. L.; Raptis, R. G.; Baran, P.; Chilas, G. I.; Sigalas, M. P.; Kabanos, T. A; Cronin, L. Solution identification and solid state characterisation of a heterometallic polyoxometalate $\{Mo_{11}V_7\}$: $[Mo^{VI}_{11}V^{V}_{5}V^{IV}_{2}O_{52}(\mu_9\text{-}SO_3)]^{7-}$. Chem. Commun. 2008, 52, 4703−4705.
(35) Maksimovskaya, R. I. Nmr Structural Aspects of the Chemistry. J. Struct Chem. 2006, 47, 952−9788.
(36) Jackson, M. N.; Kamunde-Devonish, M. K.; Hammann, B. A.; Wills, L. A.; Fullmer, L. B.; Hayes, S. E.; Cheong, P. H.-Y.; Casey, W. H.; Nyman, M.; Johnson, D. W. An overview of selected current approaches to the characterization of aqueous inorganic clusters. Dalton Trans. 2015, 44, 16982−17006.
(37) Miras, H. N.; Cronin, L. Electrospray and Cryospray Mass Spectrometry: From Serendipity to Designed Synthesis of Supra-molecular Coordination and Polyoxometalate Clusters. New Strategies in Chemical Synthesis and Catalysis 2012, 3−32.
(38) Pigga, J. M.; Kistler, M. L.; Shew, C. Y.; Antonio, M. R.; Liu, T. Counterion distribution around hydrophilic molecular macroanions: The source of the attractive force in self-assembly. Angew. Chem., Int. Ed. 2009, 48, 6538−6542.
(39) Kojima, T.; Antonio, M. R.; Ozeki, T. Solvent-driven association and dissociation of the hydrogen-bonded protonated decavanadates. J. Am. Chem. Soc. 2011, 133, 7248−7251.
(40) Yin, P.; Li, T.; Forgan, R. S.; Lydon, C.; Zuo, X.; Zheng, Z. N.; Lee, B.; Long, D.; Cronin, L.; Liu, T. Exploring the programmable assembly of a polyoxometalate-organic hybrid via metal ion coordination. J. Am. Chem. Soc. 2013, 135, 13425−13432.
(41) Goberna-Ferron, S.; Soriano-Lopez, J.; Galan-Mascaros, J. R.; Nyman, M. Solution Speciation and Stability of Cobalt-Polyoxome-talate Water Oxidation Catalysts by X-ray Scattering. Eur. J. Inorg. Chem. 2015, 2015, 2833−2840.
(42) Yin, P.; Li, T.; Forgan, R. S.; Lydon, C.; Zuo, X.; Zheng, Z. N.; Lee, B.; Long, D.; Cronin, L.; Liu, T. X-ray and Neutron Scattering Study of the Formation of Core−Shell-Type Polyoxometalates. J. Am. Chem. Soc. 2016, 138, 2638−2643.
(43) Ritchie, C.; Bryant, G. Microwave assisted synthesis of a mono organoimido functionalized Anderson polyoxometalate. Dalton Trans. 2015, 44, 20826−20829.
(44) Antonio, M. R.; Nyman, M.; Anderson, T. M. Direct observation of contact ion-pair formation in aqueous solution. Angew. Chem., Int. Ed. 2009, 48, 6136−6140.
(45) Hasenknopf, B.; Micoine, K.; Lacôte, E.; Thorimbert, S.; Malacria, M.; Thouvenot, R. Chirality in Polyoxometalate Chemistry. Eur. J. Inorg. Chem. 2008, 2008, 5001−5013.
(46) Du, D.-Y.; Yan, L.-K.; Su, Z.-M.; Li, S.-L.; Lan, Y.-Q.; Wang, E.-B. Chiral polyoxometalate-based materials: From design syntheses to functional applications. Coord. Chem. Rev. 2013, 257, 702−717.
(47) Liu, D.; Tan, H.-Q.; Chen, W.-L.; Li, Y.-G.; Wang, E.-B. Resolution of chiral polyoxoanion $[P_2Mo_{18}O_{62}]^{6-}$ with histidine. CrystEngComm 2010, 12, 2044−2046.
(48) Wang, Y.; Shi, L.; Yang, Y.; Li, B.; Wu, L. Induced circular dichroism of polyoxometalates via electrostatic encapsulation with chiral organic cations. Dalton Trans. 2014, 43, 13178−13186.
(49) Wang, Y.; Li, H.; Wu, C.; Yang, Y.; Shi, L.; Wu, L. Chiral heteropoly blues and controllable switching of achiral polyoxometalate clusters. Angew. Chem., Int. Ed. 2013, 52, 4577−4581.
(50) Kortz, U.; Savelieff, M. G.; Ghali, F. Y. A.; Khalil, L. M.; Maalouf, S. A.; Sinno, D. I. Heteropolymolybdates of As. Angew. Chem., Int. Ed. 2002, 41, 4070−4073.
(51) Naruke, H.; Iijima, J.; Sanji, T. Enantioselective Resolutions and Circular Dichroism Studies Polyoxometalates. Inorg. Chem. 2011, 50, 7535−7539.

(52) Fang, X.; Anderson, T. M.; Hill, C. L. Enantiomerically pure polytungstates: Chirality transfer through zirconium coordination centers to nanosized inorganic clusters. Angew. Chem., Int. Ed. 2005, 44, 3540−3544.

(53) Ju, W.-W.; Zhang, H.-T.; Xu, X.; Zhang, Y.; Xu, Y. Enantiomerically pure lanthanide-organic polytungstates exhibiting two-photon absorption properties. Inorg. Chem. 2014, 53, 3269−3271.

(54) Vonci, M.; Akhlaghi Bagherjeri, F.; Hall, P. D.; Gable, R. W.; Zavras, A.; O'Hair, R. A. J.; Liu, Y.; Zhang, J.; Field, M. R.; Taylor, M. B.; Du Plessis, J.; Bryant, G.; Riley, M.; Sorace, L.; Aparicio, P. A.; Lopez, X.; Poblet, J. M.; Ritchie, C.; Boskovic. Modular Molecules: Site-Selective Metal Substitution, Photoreduction, and Chirality in Polyoxometalate Hybrids. Chem. - Eur. J. 2014, 20, 14102−14111.

(55) Leyrie, M.; Martin-Frere, J.; Herve, G. Obtention et propietes de quelques tungstoarseniates(III). C. R. Acad. Sci., Ser. II 1974, 279, 895.

(56) Wassermann, K.; Pope, M. T. Large Cluster Formation through Multiple Substitution with Lanthanide Cations. Inorg. Chem. 2001, 40, 2763−2768.

(57) Chen, W.; Li, Y.; Wang, Y.; Wang, E.; Su, Z. Building block approach to nanostructures: step-by-step assembly of large lanthanide-containing polytungstoarsenate aggregates. Dalton Trans. 2007, 4293− 4301.

(58) Feng, X.-J.; Han, H.-Y.; Wang, Y.-H.; Li, L.-L.; Li, Y.-G.; Wang, E.-B. Assembly of chainlike polyoxometalate-based lanthanide complexes in one-pot reaction system. CrystEngComm 2013, 15, 7267−7273.

(59) Kortz, U.; Savelieff, M. G.; Bassil, B. S.; Dickman, M. H. A Large, Novel Polyoxotungstate: $[As^{III}_6W_{65}O_{217}(H_2O)_7]^{26-}$. Angew. Chem., Int. Ed. 2001, 40, 3384−3386.

(60) Dolomanov, O. V.; Bourhis, L. J.; Gildea, R. J.; Howard, J. A. K.; Puschmann, H. OLEX2: A complete structure solution, refinement and analysis program. J. Appl. Crystallogr. 2009, 42, 339−341.

(61) Sheldrick, G. M. SHELXT − Integrated space-group and crystal-structure determination. Acta Crystallogr. 2015, A71, 3−8.

(62) Sheldrick, G. M. Crystal structure refinement with SHELXL. Acta Crystallogr. 2015, C71, 3−8.

(63) Spek, A. L. Structure validation in chemical crystallography. Acta Crystallogr. 2009, D65, 148−155.

(64) Zuo, X.; Cui, G.; Merz, K. M.; Zhang, L.; Lewis, F. D.; Tiede, D. M. X-ray diffraction "fingerprinting" of DNA structure in solution for quantitative evaluation of molecular dynamics simulation. Proc. Natl. Acad. Sci. U. S. A. 2006, 103, 3534−3539.

(65) O'Donnell, J. L.; Zuo, X.; Goshe, A. J.; Sarkisov, L.; Snurr, R. Q.; Hupp, J. T.; Tiede, D. M. Solution-phase structural characterization of supramolecular assemblies by molecular diffraction. J. Am. Chem. Soc. 2007, 129, 1578−1585.

(66) Moore, P. B. Small-angle Scattering. Information Content and Error Analysis. J. Appl. Crystallogr. 1980, 7, 168−175.

(67) Gottlieb, H. E.; Kotlyar, V.; Nudelman, A. NMR Chemical Shifts of Common Laboratory Solvents as Trace Impurities. J. Org. Chem. 1997, 62, 7512−7515.

(68) (a) ADF2013.01; SCM, Theoretical Chemistry; Vrije Universiteit, Amsterdam, The Netherlands; http://www.scm.com. (b) Fonseca Guerra, C.; Snijders, J. G.; te Velde, G.; Baerends, E. J. Towards an order-N DFT method. Theor. Chem. Acc. 1998, 99, 391.

(c) te Velde, G.; Bickelhaupt, F. M.; Baerends, E. J.; Guerra, C. F.; van Gisbergen, S. J. A.; Snijders, J. G.; Ziegler, T. Chemistry with ADF. J. Comput. Chem. 2001, 22, 931.

(69) (a) Becke, A. D. Density functional calculations of molecular bond energies. J. Chem. Phys. 1986, 84, 4524. (b) Becke, A. D. Density-functional exchange-energy approximation with correct asymptotic behavior. Phys. Rev. 1988, A38, 3098. (c) Vosko, S. H.; Wilk, L.; Nusair, M. Accurate spin-dependent electron liquid correlation energies for local spin density calculations: a critical analysis. Can. J. Phys. 1980, 58, 1200. (d) Perdew, J. P. Phys. Rev. 1986, B33, 8822.

(e) Perdew, J. P. Perdew, Density-functional approximation for the correlation energy of the inhomogeneous electron gas. Phys. Rev. 1986, B34, 7406.

(70) (a) Klamt, A.; Schüürmann, G. COSMO: a new approach to dielectric screening in solvents with explicit expressions for the screening energy and its gradient. J. Chem. Soc., Perkin Trans. 2 1993, 2, 799. (b) Andzelm, J.; Kölmel, C.; Klamt, A. Incorporation of solvent effects into density functional calculations of molecular energies and geometries. J. Chem. Phys. 1995, 103, 9312. (c) Klamt, A. Conductor-like Screening Model for Real Solvents: A New Approach to the Quantitative Calculation of Solvation Phenomena. J. Phys. Chem. 1995, 99, 2224. (d) Pye, C. C.; Ziegler, T. An implementation of the conductor-like screening model of solvation within the Amsterdam density functional package. Theor. Chem. Acc. 1999, 101, 396.

(71) Brown, I. D. The Chemical Bond in Inorganic Chemistry: The Bond Valence Model; Oxford University Press: Oxford, England, 2002.

(72) Brown, I. D.; Altermatt, D. Bond-Valence Parameters Obtained from a Systematic Analysis of the Inorganic Crystal Structure Database. Acta Crystallogr. 1985, B41, 244−247.

(73) Vonci, M.; Boskovic, C. Unpublished results.

(74) Thouvenot, R.; Fournier, M.; Franck, R.; Rocchiccioli-Deltcheff, C. Vibrational investigations of polyoxometalates. 3. Isomerism in molybdenum(VI) and tungsten(VI) compounds related to the Keggin structure. Inorg. Chem. 1984, 23, 598−605.

(75) Way, D. M.; Cooper, J. B.; Sadek, M.; Vu, T.; Mahon, P. J.; Bond, A. M.; Brownlee, R. T. C.; Wedd, A. G. Systematic Electrochemical Synthesis of Reduced Forms of the alpha-$[S_2Mo_{18}O_{62}]^{4-}$ Anion. Inorg. Chem. 1998, 37, 604−613.

(76) Garvey, J. F.; Pope, M. T. Chirality of oxidized and reduced octadecamolybdodiphosphate anions. Observation of a Pfeiffer effect. Inorg. Chem. 1978, 17, 1115−1118.

(77) Sun, H.-R.; Zhang, S.-Y.; Xu, J.-Q.; Yang, G.-Y.; Shi, T.-S. J. Electrochemical and in-situ UV-visible-near-IR and FTIR spectroelec-trochemical characterisation of the mixed-valence heteropolyanion $PMo_{12}O_{40}^{n-}$ (n = 4, 5, 6, 7) in aprotic media. J. Electroanal. Chem. 1998, 455, 57−68.

(78) Fournier, M.; Rocchiccioli-Deltcheff, C.; Kazansky, L. P. Infrared spectroscopic evidence of bipolaron delocalization in reduced heterododecamolybdates. Chem. Phys. Lett. 1994, 223, 297−300.

(79) Boskovic, C.; Sadek, M.; Brownlee, R. T. C.; Bond, A. M.; Wedd, A. G. Electrosynthesis and solution structure of six-electron reduced forms of metatungstate, $[H_2W_{12}O_{40}]^{6-}$. J. Chem. Soc., Dalton Trans. 2001, 187−196.

(80) Fleisch, T. H. An XPS study of the UV reduction and photochromism of MoO_3 and WO_3. J. Chem. Phys. 1982, 76, 780−786.

(81) Feng, W.; Ding, Y.; Liu, Y.; Lu, R. The photochromic process of polyoxometalate-based nanocomposite thin film by in situ AFM and spectroscopy. Mater. Chem. Phys. 2006, 98, 347−352.

(82) Wang, L.; Yin, P.; Zhang, J.; Hao, J.; Lv, C.; Xiao, F.; Wei, Y. X-octamolybdate $[Mo^{V}_4Mo^{VI}_4O_{24}]^{4-}$: An unusual small polyoxometalate in partially reduced form from nonaqueous solvent reduction. Chem. - Eur. J. 2011, 17, 4796−4801.

(83) Zhang, J.; Li, W.; Wu, C.; Li, B.; Zhang, J.; Wu, L. Redox-controlled helical self-assembly of a polyoxometalate complex. Chem. - Eur. J. 2013, 19, 8129−8135.

(84) Sanchez, C.; Livage, J.; Launay, J. P.; Fournier, M.; Jeannin, Y. Electron Delocalization in Mixed-Valence Molybdenum. J. Am. Chem. Soc. 1982, 104, 3194−3202.

(85) Sanchez, C.; Livage, J.; Launay, J. P.; Fournier, M. Electron Delocalization in Mixed-Valence Tungsten. J. Am. Chem. Soc. 1983, 105, 6817−6823.

(86) Duncan, D. C.; Hill, C. L. Synthesis and Characterization of the Mixed-Valence Diamagnetic Two-Electron-Reduced Isopolytungstate $[W_{10}O_{32}]^{6-}$. Evidence for an Asymmetric d-Electron Distribution over the Tungsten Sites. Inorg. Chem. 1996, 35, 5828−5835.

(87) Yin, P.; Li, D.; Liu, T. Solution behaviors and self-assembly of polyoxometalates as models of macroions and amphiphilic polyox-ometalate-organic hybrids as novel surfactants. Chem. Soc. Rev. 2012, 41, 7368−7383.

(88) Knoppe, S.; Dharmaratne, A. C.; Schreiner, E.; Dass, A.; Bürgi, T. Ligand Exchange Reactions on Au_{38} and Au_{40} Clusters: A

Combined Circular Dichroism and Mass Spectrometry Study. J. Am. Chem. Soc. 2010, 132, 16783−16789.

(89) Amdursky, N.; Stevens, M. M. Circular Dichroism of Amino Acids: Following the Structural Formation of Phenylalanine. ChemPhysChem 2015, 16, 2768−2774.

(90) Schaffer, C.; Merca, A.; Bögge, H.; Todea, A. M.; Kistler, M. L.; Liu, T.; Thouvenot, R.; Gouzerh, P.; Müller, A. Unprecedented and differently applicable pentagonal units in a dynamic library: a keplerate of the type $\{(W)W_5\}_{12}\{Mo_2\}_{30}$. Angew. Chem., Int. Ed. 2009, 48, 149− 153.

(91) Grego, A.; Müller, A.; Weinstock, I. A. Stepwise-resolved thermodynamics of hydrophobic self-assembly. Angew. Chem., Int. Ed. 2013, 52, 8358−8362.

(92) Müller, A.; Gouzerh, P. Capsules with highly active pores and interiors: versatile platforms at the nanoscale. Chem. - Eur. J. 2014, 20, 4862−4873.

(93) Doddrell, D.; Allerhand, A. Segmental motion in liquid 1-decanol. Application of natural-abundance carbon-13 partially relaxed Fourier transform nuclear magnetic resonance. J. Am. Chem. Soc. 1971, 93, 1558−1559.

(94) Yan, L.; Lopez, X.; Carbo, J. J.; Sniatynsky, R.; Duncan, D. C.; Poblet, J. M. On the origin of alternating bond distortions and the emergence of chirality in polyoxometalate anions. J. Am. Chem. Soc. 2008, 130, 8223−8233.

(95) Lopez, X.; Bo, C.; Poblet, J. M. Electronic Properties of Polyoxometalates: Electron and Proton Affinity of Mixed-Addenda Keggin and Wells - Dawson Anions. J. Am. Chem. Soc. 2002, 124, 12574−12582.

(96) Parent, L.; Aparicio, P. A.; De Oliveira, P.; Teillout, A. L.; Poblet, J. M.; Lopez, X.; Mbomekalle, I. M. Effect of electron (De) localization and pairing in the electrochemistry of polyoxometalates: Study of Wells-Dawson molybdotungstophosphate derivatives. Inorg. Chem. 2014, 53, 5941−5949.

(97) Lopez, X.; Fernandez, J. A.; Poblet, J. M. Redox properties of polyoxometalates: new insights on the anion charge effect. Dalton Trans. 2006, 1162−1167.